Environmental Factors in the Upscale Growth and Longevity of MCSs Derived from Rapid Update Cycle Analyses

MICHAEL C. CONIGLIO, JASON Y. HWANG, AND DAVID J. STENSRUD

NOAA/National Severe Storms Laboratory, Norman, Oklahoma

(Manuscript received 18 September 2009, in final form 20 April 2010)

ABSTRACT

Composite environments of mesoscale convective systems (MCSs) are produced from Rapid Update Cycle (RUC) analyses to explore the differences between rapidly and slowly developing MCSs as well as the differences ahead of long- and short-lived MCSs. The composite analyses capture the synoptic-scale features known to be associated with MCSs and depict the inertial oscillation of the nocturnal low-level jet (LLJ), which remains strong but tends to veer away from decaying MCSs. The composite first storms environment for the rapidly developing MCSs contains a stronger LLJ located closer to the first storms region, much more conditional instability, potential instability, and energy available for downdrafts, smaller 3–10-km vertical wind shear, and smaller geostrophic potential vorticity in the upper troposphere, when compared to the environment for the slowly developing MCSs. The weaker shear above 3 km for the rapidly developing MCSs is consistent with supercell or discrete cell modes being less likely in weaker deep-layer shear and the greater potential for a cold pool to trigger convection when the shear is confined to lower levels. Furthermore, these results suggest that low values of upper-level potential vorticity may signal a rapid transition to an MCS. The composite environment ahead of the genesis of long-lived MCSs contains a broader LLJ, a better-defined frontal zone, stronger low-level frontogenesis, deeper moisture, and stronger wind shear above 2 km, when compared to short-lived MCSs. The larger shear above 2 km for the long-lived MCSs is consistent with the importance of shear elevated above the ground to help organize and maintain convection that feeds on the elevated unstable parcels after dark and is indicative of the enhanced baroclinicity ahead of the MCSs.

1. Introduction

Organized clusters of thunderstorms and their cold outflows that meet particular spatial and temporal requirements have been termed mesoscale convective systems (MCSs; e.g., Zipser 1982; Hilgendorf and Johnson 1998; Parker and Johnson 2000) and are important because of their propensity to produce excessive rainfall (Maddox et al. 1979; Fritsch et al. 1986; Augustine and Caracena 1994; Moore et al. 2003; Schumacher and Johnson 2009) and severe weather (Johns 1984; Johns and Hirt 1987; Ashley and Mote 2005). There are many organizational modes of MCSs (Parker and Johnson 2000; Jirak and Cotton 2003), but this study focuses on the type that are of particular importance to severe-weather forecasting (i.e., those that move or propagate in the general direction of the mean wind and maintain strong convection along their leading edge).

The mode of convection (i.e., its organizational characteristics) and the duration of the convective episode are two important aspects of severe weather forecasting. The goal of this study is to address these difficult forecast problems as they apply to two aspects of MCS evolution: the speed at which MCSs develop and the longevity of MCSs. The motivation for wanting to differentiate rapidly from slowly developing MCSs is driven by the relationship between the type of severe weather produced and the dominant convective mode. Many types of severe weather (e.g., large hail, significant tornadoes, severe convective winds) are possible with supercell or discrete convective modes, but it is known that the likelihood of large hail and significant tornadoes decreases and the threat for severe convective winds (and more widespread flash flooding) increases as the convection transitions to an MCS (Johns and Doswell 1992; Gallus et al. 2008). Therefore, an

Corresponding author address: Dr. Michael C. Coniglio, National Severe Storms Laboratory, National Weather Center, Room 2234, 120 David L. Boren Blvd., Norman, OK 73072.
E-mail: michael.coniglio@noaa.gov

DOI: 10.1175/2010MWR3233.1

environment that is favorable for a rapid transition to an MCS may shorten the duration of the threat for large hail and significant tornadoes and increase the threat of more widespread severe surface winds. It follows that the recognition of the environments favorable for a rapidly developing MCS could lead to more accurate forecasts of the timing of upscale transition and the type of severe weather produced during the convective event.

If a transition into an MCS takes place, forecasters then need to address the problem of how long the MCS will last. By definition, all events in this study eventually grow upscale into quasi-linear systems (see section 2 for the criteria used to define the MCSs in this study). Understanding the longevity of these types of MCSs is important for making accurate short-term prediction of the geographical extent and duration of severe weather and for the difficult problem of forecasting heavy rainfall over regional areas that can lead to flash flooding (Schumacher and Johnson 2005).

This study uses the hourly three-dimensional analyses of the Rapid Update Cycle (RUC) model (Benjamin et al. 2004) provided on a 20-km grid to examine MCS environments. RUC model output has been used effectively in a similar capacity to study both supercells (Thompson et al. 2003) and MCSs (Schumacher and Johnson 2005; Hane et al. 2008; Schumacher and Johnson 2009). An obvious benefit of the RUC analyses is that the 20-km horizontal grid provides the ability to probe mesoscale features of the environment. Another benefit is that the hourly update of the analysis allows the environments to be examined at times other than the nominal radiosonde times of 0000 and 1200 UTC, which often encompasses the time that MCSs develop and mature (Maddox 1983; Cotton et al. 1989; Evans and Doswell 2001). Root-mean-square fits of the RUC analyses to rawinsonde observations and surface observations are generally of similar magnitude to measurement accuracy (Thompson et al. 2003; Benjamin et al. 2004; Hane et al. 2008).

Variables that could be used to improve forecasts of MCS evolution are highlighted through MCS-relative composites of the RUC analyses. A unique aspect of this study is the presentation of the spatial distribution of both the mean variables and the statistical significance of the differences in the variables between MCS subsets. The data selection procedures and the methodology for analyzing the RUC analyses are presented in section 2. Section 3 presents composite MCS environments that illustrate features important to the upscale growth and longevity of MCSs and incorporates past studies of MCS environments into the discussion. A summary and discussion is given in section 4.

2. Data and methodology

a. Identification and classification of MCS events

Images from the WSI Corporation National Operational Weather radio (NOWrad) 2-km national composite of the Weather Surveillance Radar-1988 Doppler (WSR-88D) network at approximately half-hour intervals are examined for the months of May–August for the years 2005–08 to identify MCS events. An MCS must obtain a nearly contiguous region of reflectivity $\geq$35 dBZ at least 100 km in length and contain some embedded echoes $\geq$50 dBZ for at least 5 continuous hours to be considered in this study. Of the many forms of organized convection that can be considered to be an MCS (Anderson and Arritt 1998; Parker and Johnson 2000; Jirak and Cotton 2003), these criteria ensure that only the more robust forms of MCSs are examined in this study, similar to those examined in Coniglio et al. (2007), Cohen et al. (2007), and Engerer et al. (2008). Although the initial structures for some of the MCSs in this dataset resemble the trailing-line/adjoining-stratiform archetype commonly associated with heavy-rain producing MCSs (Schumacher and Johnson 2005) or the parallel or leading stratiform MCS archetypes (Parker and Johnson 2000), all of the MCSs eventually transition into a structure that resembles the leading-line–trailing-stratiform conceptual model of midlatitude eastward-advancing MCSs (Houze et al. 1989).

Each MCS is categorized subjectively into five stages: 1) first storms, 2) genesis, 3) mature, 4) decay, and 5) dissipation (see Fig. 1 for an example of these definitions for an MCS that occurred on 9–10 June 2005). The time of the first storms is defined as the first hour prior to the appearance of the first echo that eventually becomes part of the MCS, and thus the environment during the first storms stage can be viewed as being preconvective. The genesis stage occurs at the first full hour after the individual convective cells merge into a continuous convective line or arc at least 100 km in length. The mature stage is defined at a time when the MCS has a nearly contiguous convective line or arc with a well-defined stratiform precipitation region that occurs at least 2 h after the genesis stage and at least 2 h before the decay stage. The decay stage is defined at the first full hour before the reflectivity associated with the leading convective line begins to decrease and the line becomes less cohesive with time. The dissipation stage is defined at the first full hour before a leading convective line is no longer observed.

A total of 94 MCSs are identified between 2005 and 2008 that meet the established criteria (Fig. 2). A latitude–longitude point of the first storms is defined for the first storms stage, and a location near the center of the leading

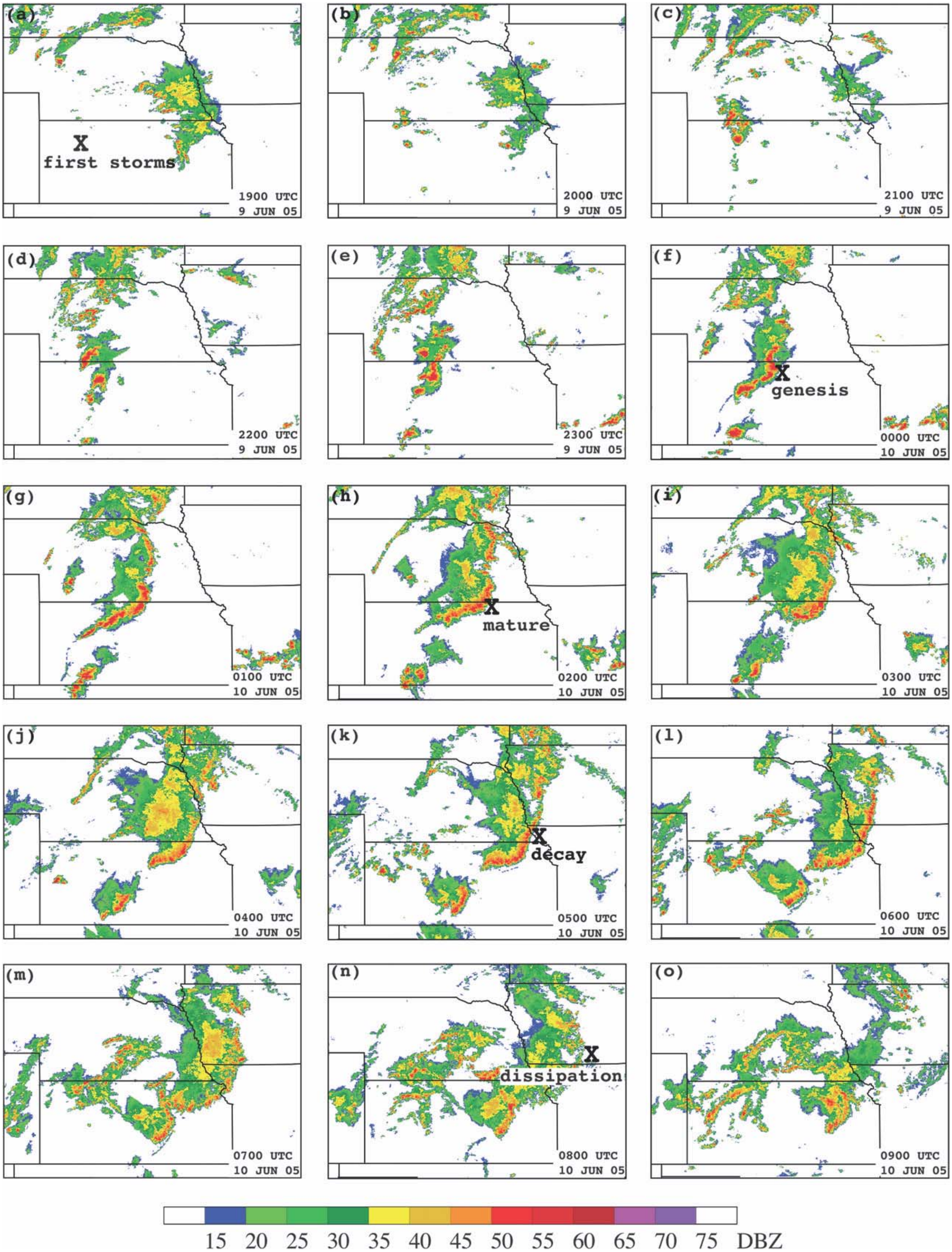

FIG. 1. Hourly composite reflectivity images exemplifying the five stages of MCSs used in this study for the 9–10 Jun 2005 MCS event: (a) first storms, (f) genesis, (h) mature, (k) decay, and (n) dissipation stages. Courtesy of the WSI NOWrad composite reflectivity data.

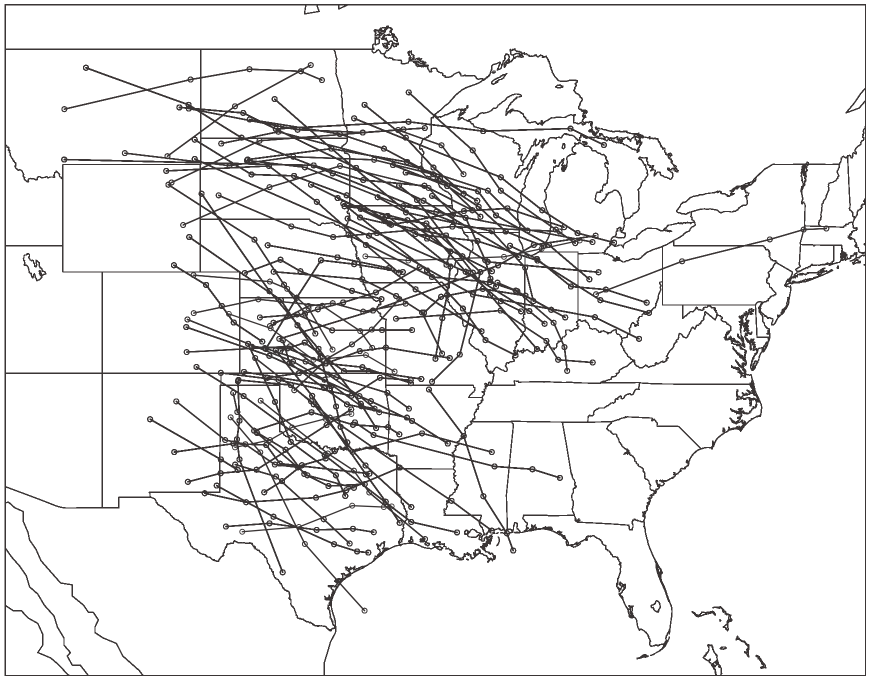

FIG. 2. Paths of the 94 MCSs used in this study. The open circles denote the location of the first storms, genesis, mature, decay, and dissipation stages, respectively.

edge of the convective line is determined for each of the four remaining MCS stages. A mean storm motion is calculated for each stage by using the distance between the latitude–longitude points defined for each stage. The time elapsed between the stages is used to calculate the storm speed and the angle between the latitude of the first latitude–longitude point and a vector between the two latitude–longitude points is used to calculate the storm direction. The MCS direction of motion for each stage is used to develop MCS-relative composite analyses as described next.

b. Data for examining MCS environments

The environmental characteristics of the 94 MCSs are derived from the hourly RUC model analyses provided on a 20-km grid and on constant pressure surfaces spaced 25 hPa apart. For each case and for each MCS stage, variables derived from the RUC analyses are mapped to a common grid consisting of 81 by 61 grid points with 20-km grid spacing (1600 km by 1200 km) with the center of the grid located at the latitude–longitude points described above and the long axis of the grid (x direction) aligned with the MCS motion vector. The wind components are rotated to this MCS-relative coordinate system to preserve the orientation of the flow features for the purposes of the compositing procedure.

Mean MCS-relative composites are examined first to determine if the RUC analyses capture features that are known to be important in MCS evolution, thereby providing confidence in this method to examine MCS environments in detail. Furthermore, the Wilcoxon–Mann–Whitney (WMW) test (Wilks 1995) is used to assess the significance of the differences in the environments between subsets of the 94 MCSs, as done similarly for observed MCS proximity soundings in Coniglio et al. (2007) and Cohen et al. (2007). The WMW test allows one to use the Gaussian distribution on the test statistic to assess the confidence in the differences, even though the parent distribution may not be Gaussian. Thus, it is much more resistant to outliers and parametric errors than the widely used Student's t test (see Wilks 1995 for details). Furthermore, nonparametric tests like the WMW test are preferred over the t test because the data distributions are not known a priori, which needs to be assumed in the t test. The standard Gaussian variables of the differences, and the associated probabilities that their distributions are different, are calculated at each grid point (using the number of cases in each subset as the effective degrees of freedom) and then contoured to give a depiction of the spatial distribution of the significance of the differences. This procedure allows for an identification of the significant environmental features that distinguish MCS types. Knowledge of these features present in the RUC analysis could aid in the forecasting of MCSs.

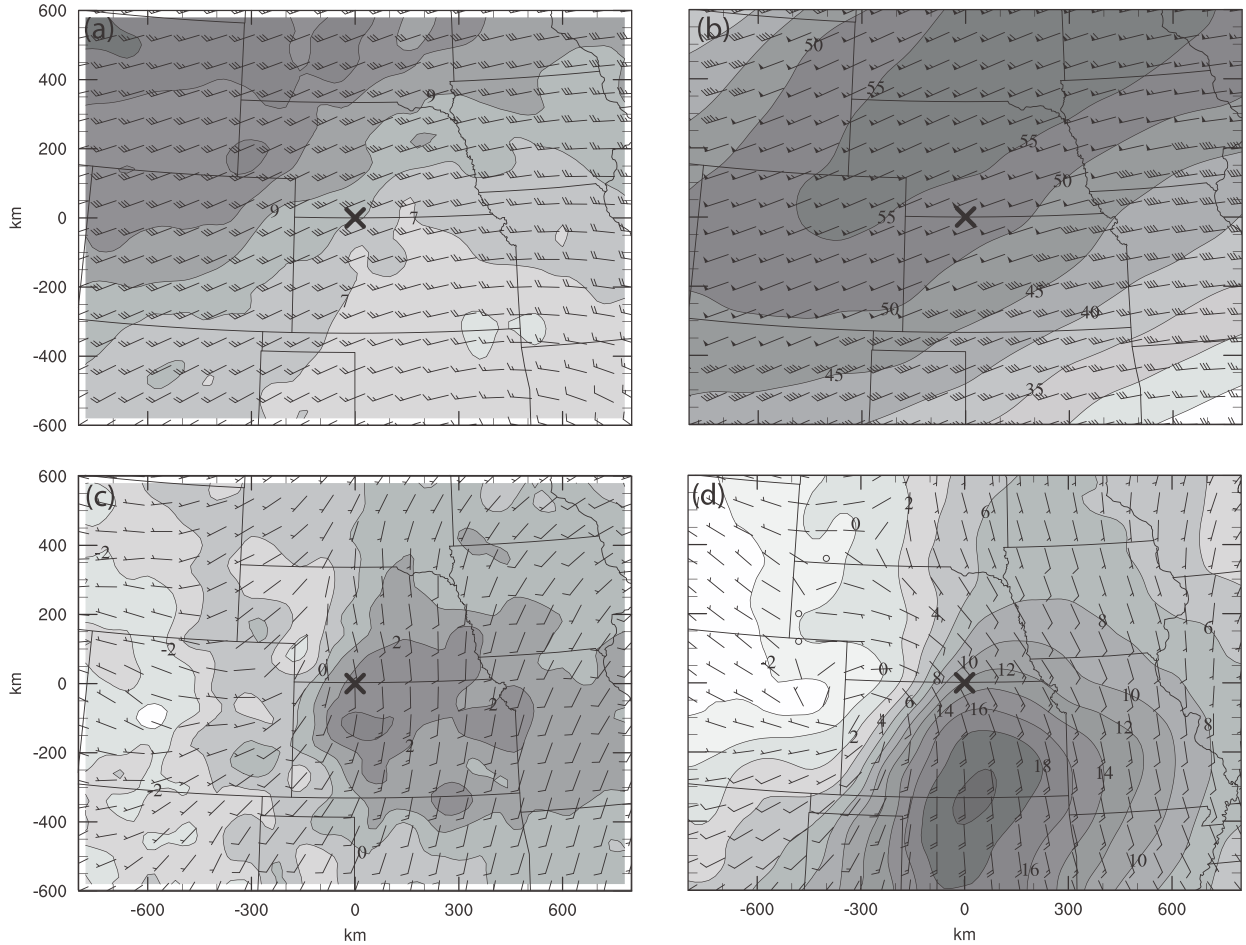

FIG. 3. Mean analyses of (a) absolute vorticity (10^{-5} s^{-1}) at 500 hPa, (b) wind speed (kt) at 200 hPa, and (c) temperature advection at 850 hPa (K 12 h^{-1}) for the first storms stage. (d) Contours of mean wind speed normal to MCS motion (kt) at 500 m AGL for the genesis stage. Barbs are drawn every 5 kt with half (full) barbs starting at 2.5 (7.5) kt. The composites in (a),(b), and (c) are relative to the location of the first storms (indicated by the X) and are relative to the location of the center of the MCS leading line for the genesis stage in (d) (also denoted by the X). The map background is shown for scale reference only.

3. Results

a. Mean MCS-relative composites

The mean composites averaged over the first storms stage for all 94 MCS cases reveal synoptic-scale features that are known to be associated with the development of MCSs (Fig. 3). An area of mean 500-hPa cyclonic vorticity advection near the first storms region (Fig. 3a) results from the averaging of upstream short-wave troughs in the individual analyses. In addition, the first storms tend to develop in the right-rear quadrant of an upper-level wind maximum (Fig. 3b) and on the western edge of low-level warm advection (Fig. 3c), in agreement with many past studies of MCS environments (e.g., Maddox 1983; Cotton et al. 1989; Johns 1993; Coniglio et al. 2004; Jirak and Cotton 2007).

As expected, given the high proportion of nocturnal systems in the central United States in this dataset (Fig. 2), the MCS genesis tends to occur on the western edge of a low-level wind maximum (Fig. 3d). The composites capture the nocturnal inertial oscillation of the low-level wind (Blackadar 1957) associated with the Great Plains low-level jet (LLJ; Bonner 1968; Fig. 4). The mean ageostrophic wind has a significant component toward the MCS genesis region (Fig. 4a), consistent with the early stages of the nocturnal boundary layer decoupling from the free atmosphere above (McNider and Pielke 1981). Furthermore, the mean component of the ageostrophic wind normal to the MCS motion strengthens ahead of MCS maturity (cf. Figs. 4b,d), signaling the nighttime strengthening of the southerly LLJ. In addition, the mean component of the ageostrophic wind parallel to the MCS

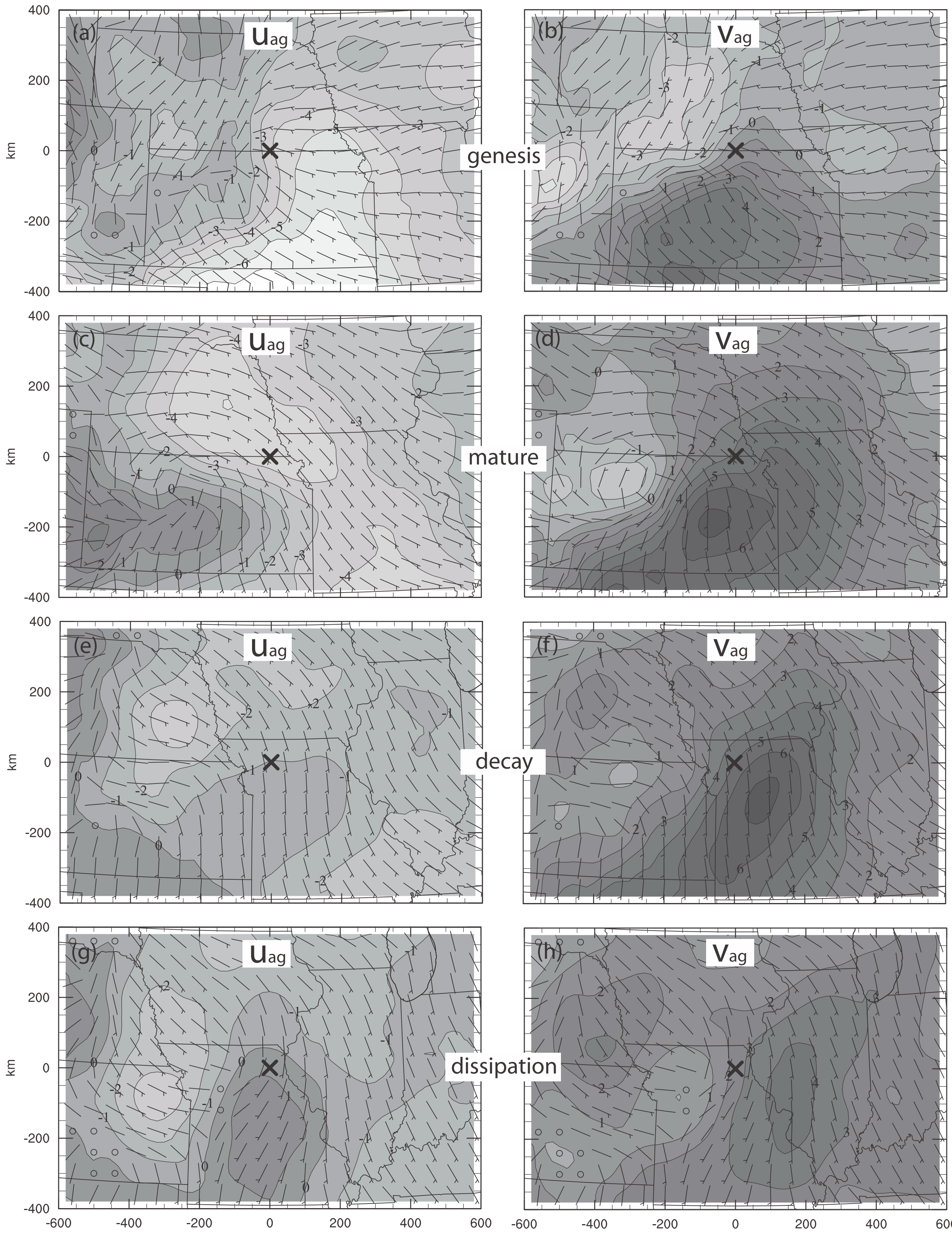

FIG. 4. The component of the 900-hPa ageostrophic winds (left) parallel to the MCS motion (u_{ag}) shaded and contoured every 1 kt and (right) normal to the MCS motion (v_{ag}) shaded and contoured every 1 kt for the (from top to bottom) MCS genesis, mature, decay, and dissipation stages. Barbs denote the ageostrophic wind vector with barbs drawn every 5 kt with half (full) barbs starting at 2.5 (7.5) kt.

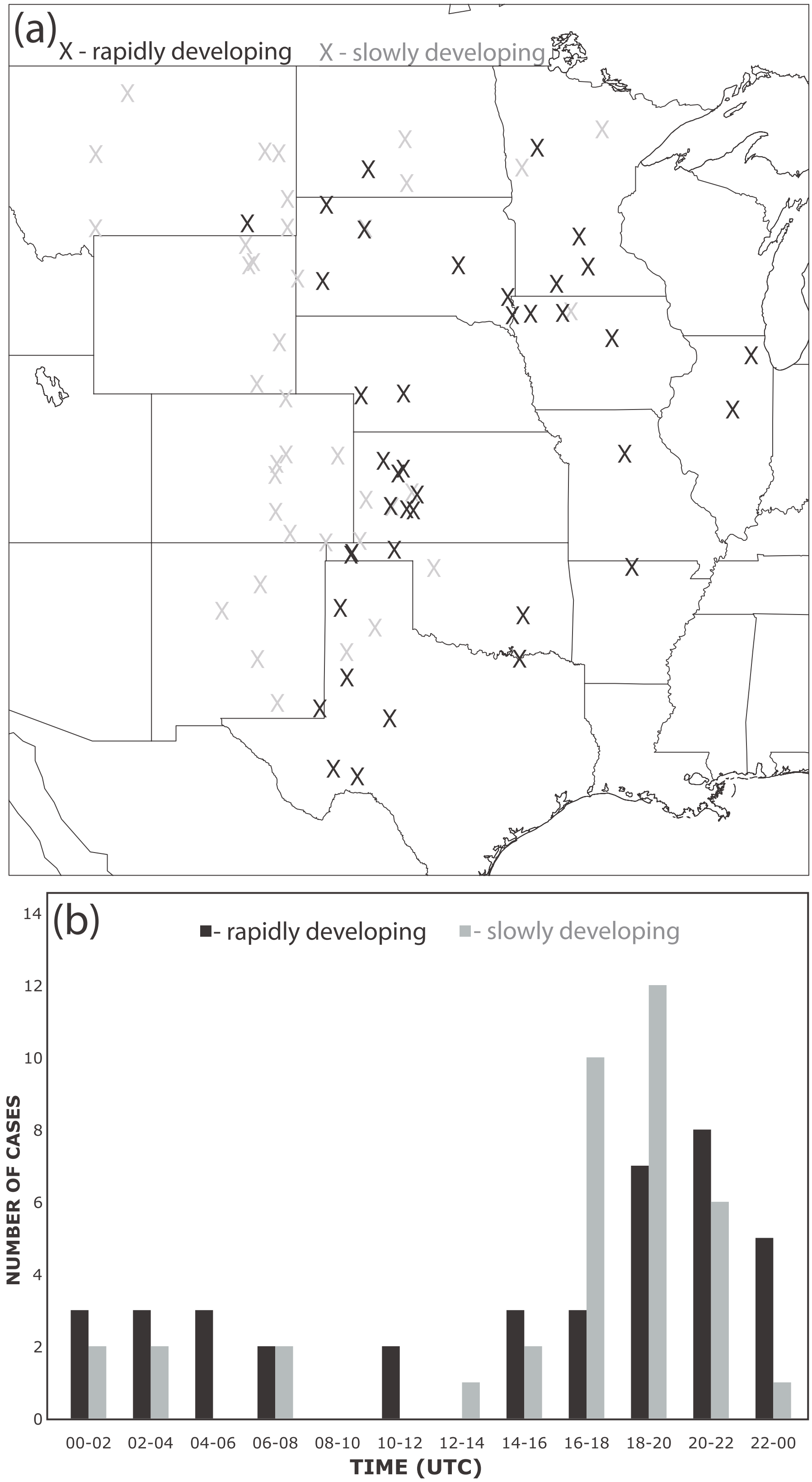

FIG. 5. (a) The location of the first storms for the RDMs (black) and SDMs (gray). (b) Histogram of the time (UTC) of the first storms for the RDMs (black) and SDMs (gray).

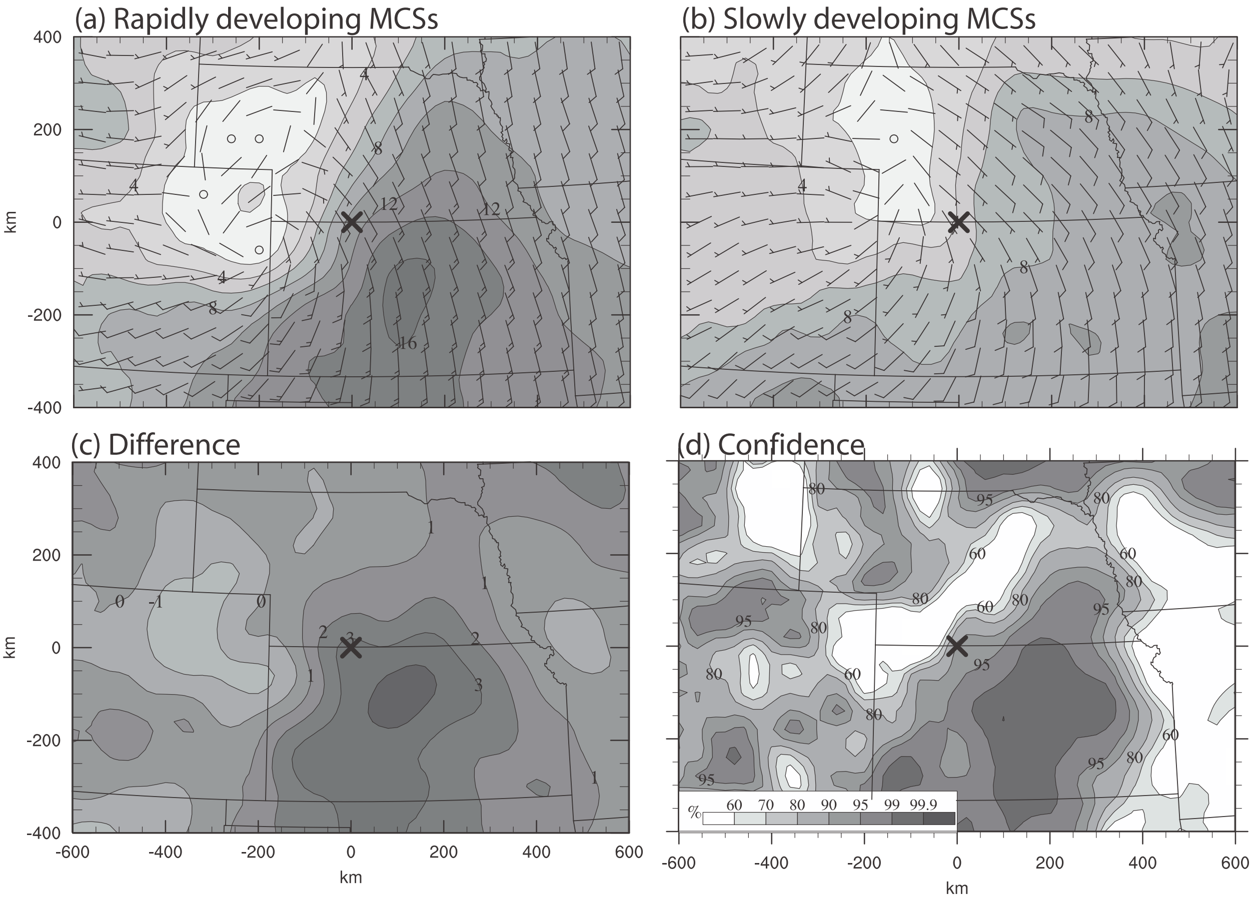

FIG. 6. The mean 500 m AGL wind speed (kt) for the (a) 39 rapidly developing MCSs, (b) the 38 slowly developing MCSs shaded and contoured every 2 kt, (c) the difference in the means between the fast-developing and slow-developing MCSs shaded and contoured every 1 kt, and (d) contours of the confidence that the distributions are different based on the WMW test (see text for details). Barbs denote the 500 m AGL total wind vector with half (full) barbs starting at 2.5 (7.5) kt.

motion continues to have a significant component toward the MCS during the mature stage (Fig. 4c).

It is interesting that ahead of decaying MCSs, the normal component of the ageostrophic wind maintains its magnitude and broadens slightly, but the parallel component nearly vanishes (Fig. 4e). This shows that the LLJ often does not lose its strength as the leading convective line of the MCS begins to decay, but a key factor in the demise of the convective line is the veering of the winds such that the component of the ageostrophic wind parallel to the MCS motion almost vanishes. This suggests that the decrease in storm-relative inflow and convergence along the leading edge of decaying MCSs (Evans and Doswell 2001; Gale et al. 2002; Coniglio et al. 2004) is related more to the tendency of the LLJ to veer with time than to a decrease in the overall intensity of the LLJ. The overall dissipation of the MCS, however, is marked both by a continued veering of the LLJ and a weakening of the LLJ intensity (Figs. 4g,h). The fact that the composites capture mesoscale features of the LLJ known to be important in MCS evolution gives confidence to the interpretation of other mesoscale features in the composite analyses in the following sections.

b. *Environmental factors in the speed of upscale growth*

Potential key environmental factors influencing the speed of the transition from initial cells to an MCS are examined through a comparison of the environments between MCSs that develop rapidly versus those that develop slowly. As mentioned earlier, the anticipation of environments that favor a rapid transition to an MCS could provide confidence that the severe weather threat will shift more quickly from large hail and significant tornadoes to severe convective winds. The 39 MCSs for which the time between the first storms and genesis stage is $\leq$5 h [i.e., the rapidly developing MCSs (RDMs)] is compared to a set of 38 MCSs for which the time between

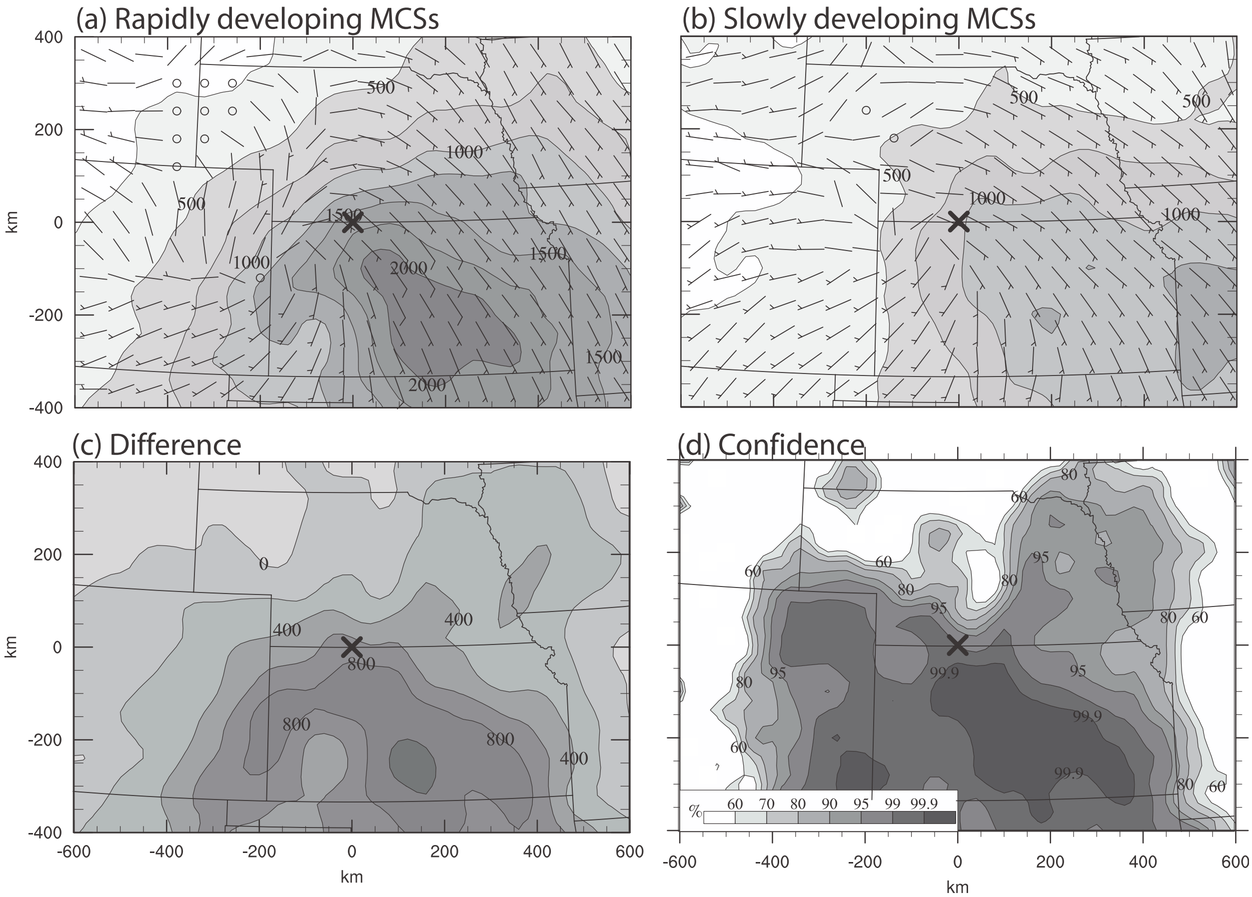

FIG. 7. As in Fig. 6, but a comparison of mean CAPE (J kg^{-1}) and 10-m wind vectors between the RDMs and SDMs. A hybrid most-unstable–mixed parcel is used to calculate the CAPE as follows: at every 50 hPa in the vertical, the CAPE is calculated using a parcel with a wet-bulb potential temperature that results from averaging the temperature and water vapor mixing ratio over the neighboring 100-hPa layer. The resulting CAPE in the figure is the maximum of those calculations.

the first storms and genesis stage is ≥7 h [i.e., the slowly developing MCSs (SDMs)]. The sensitivity of the results to these definitions was examined by recomputing the statistics for the variables shown below for the 23 MCSs for which the time between the first storms and genesis stage is ≤4 h and the 27 MCSs for which the time between the first storms and genesis stage is ≥8 h. The qualitative interpretation of the comparison described below does not change for any of the variables with these more restrictive criteria, which increases our confidence in the generality of the results. In fact, the quantitative differences actually increase for most of the variables, but we used the time differences of 5 and 7 h in most of the illustrations shown below because of the larger sample sizes and the more meaningful statistics.

1) Low-level jet and thermodynamic instability

There is no appreciable difference in the monthly distributions between the RDMs and SDMs, but the first storms for the SDMs tend to form closer to the mountains of the west-central United States and earlier in the day compared to the RDMs (Fig. 5). Since the LLJ is known to undergo rapid evolution during the late afternoon and late evening hours (McNider and Pielke 1981), it is not surprising that the mean LLJ is found to be significantly stronger and tends to be located closer to the first storms region for the RDMs (Fig. 6). The development of deep convection in proximity to a strengthening LLJ is therefore a key factor in the speed of MCS development.

Results show that the RDMs develop in environments with significantly *smaller* lapse rates than the SDMs in both low and midlevels (not shown), likely because the first storms for the SDMs are located nearer to elevated mixed-layer air over the higher terrain (Lanicci and Warner 1991) and tend to occur closer to the time of peak heating (Fig. 5). However, the smaller lapse rates for the RDMs do not translate into smaller conditional instability for updraft parcels or smaller potential energy

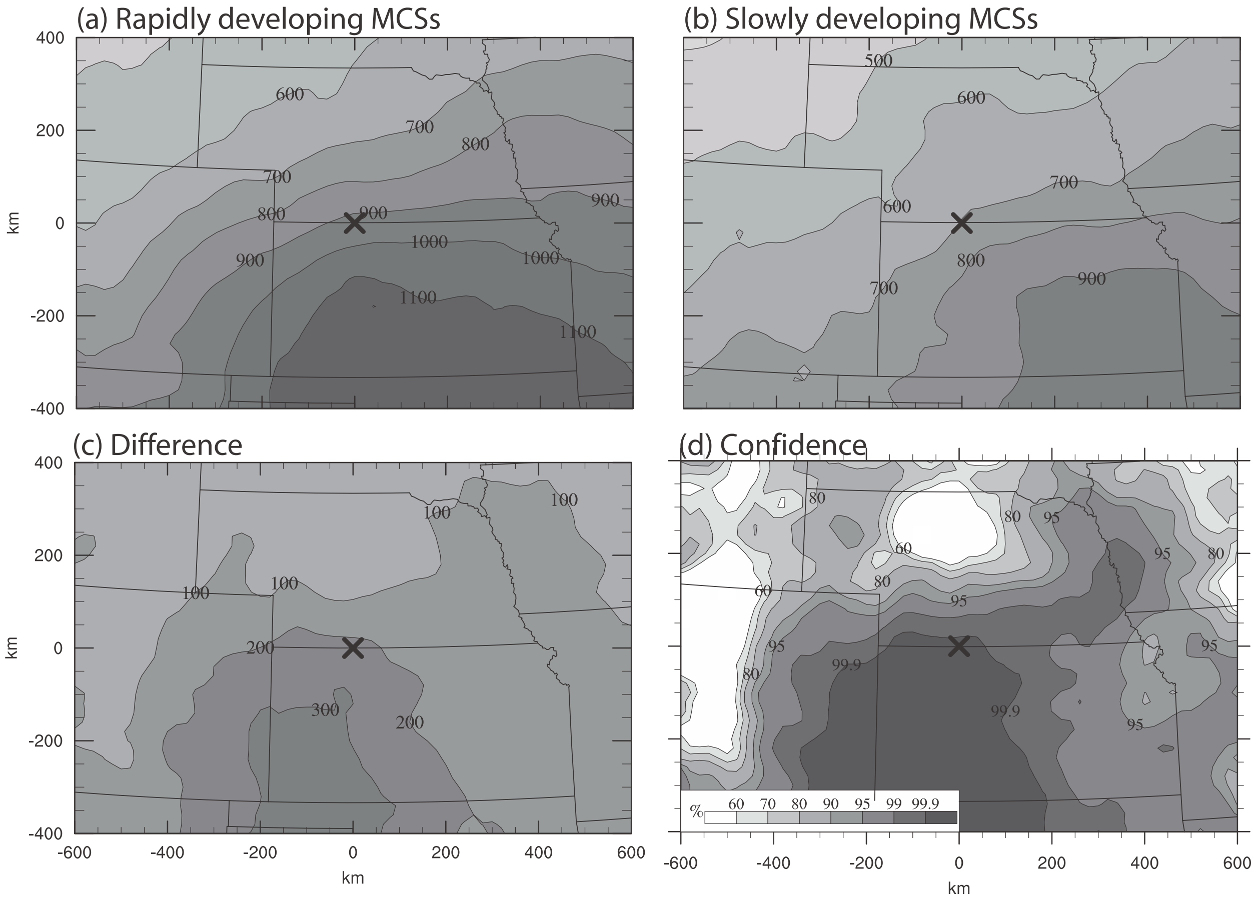

FIG. 8. As in Fig. 6, but a comparison of DCAPE (J kg^{-1}) between the RDMs and SDMs.

for downdraft parcels. In fact, both the convective available potential energy (CAPE) and downdraft CAPE[1] (DCAPE) are significantly larger for the RDMs in a broad area encompassing the first storms region (Figs. 7 and 8). The larger CAPE is a result of the higher low-level θ_e and the larger DCAPE is related to lower θ_e in midlevels (near the wet-bulb zero height).

The disparity in the vertical profile of θ_e between the RDMs and SDMs is seen in a comparison of potential instability ($\partial\theta_e/\partial z < 0$) (Fig. 9), which shows much larger magnitudes for the RDMs. It is important to note that the large differences in CAPE and DCAPE (Figs. 7 and 8) are likely very important here—more instability available for updrafts increases the potential for strong convection and strong, cold downdrafts. However, the larger potential instability for the RDMs suggests two additional factors may be important. First, large potential instability can help maintain or enhance downdrafts that remain saturated (Proctor 1989; Atkins and Wakimoto 1991) because the larger ambient *virtual* temperatures in low levels allows the differences in virtual temperatures between the negatively buoyant of downdraft parcels and the ambient air to be maintained more so than would otherwise occur in drier low levels. Second, large potential instability can facilitate rapid destabilization when entire layers of air undergo strong lifting. This type of so-called slabular lifting is known to occur along strong cold pools (Bryan and Fritsch 2000), which often occurs with MCSs with significant line-normal wind shear and storm-relative inflow (James et al. 2005). An environment that encourages slabular lifting (i.e., an environment with large potential instability) could encourage a more rapid ‘‘filling in’’ of strong convection along the cold pool, and hence, a more rapid transition to an MCS. Dry, subcloud layers and large temperature lapse rates associated with deep, well-mixed boundary layers are important for the development of organized cold pools in many convective situations (Srivastava 1985; Wakimoto 1985; Corfidi et al. 2006). But since the temperature lapse rates were *smaller* for the RDMs, the above results

[1] DCAPE is calculated using the thermodynamic properties of the parcel starting from the wet-bulb zero height.

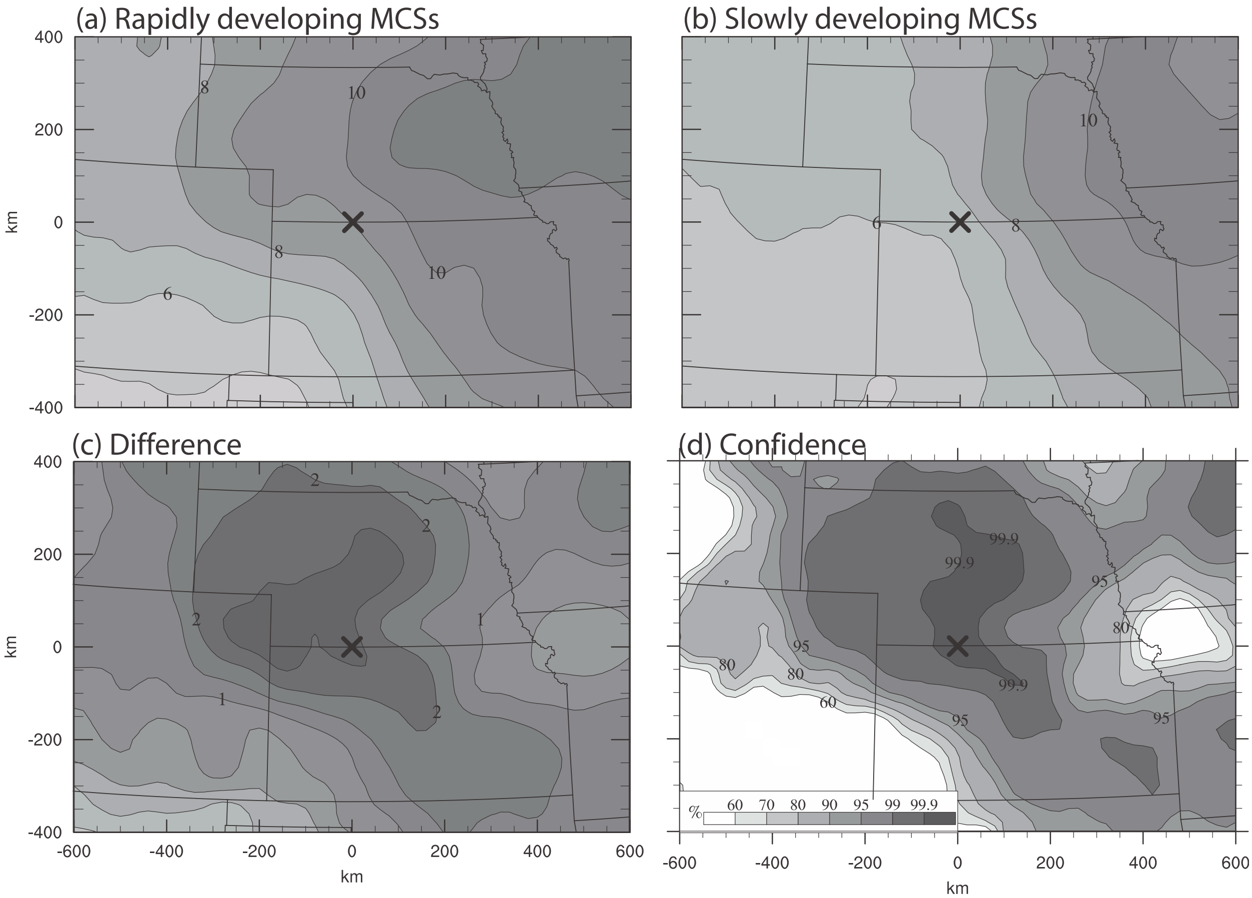

FIG. 9. As in Fig. 6, but a comparison of the difference in equivalent potential temperature (K) between 500 and 3000 m AGL between the RDMs and SDMs.

suggest that the cold pools and the subsequent MCSs in this dataset develop rapidly more so because of the large CAPE and large potential instability in the environment rather than the existence of well-mixed subcloud layers.

2) Inertial instability

Emanuel (1979), Blanchard et al. (1998), and others argue that weak inertial stability (or instability) in the upper troposphere can encourage the growth of meso-β-scale convective elements that often precede the development of MCSs (McAnelly et al. 1997; Jirak and Cotton 2003). Under inertial instability, the momentum fields are susceptible to strongly divergent mesoscale circulations and can act as an efficient ventilation mechanism for the convective updrafts. Inertial instability is usually diagnosed in a parcel theory framework in geostrophic flow (Bennetts and Hoskins 1979; Emanuel 1979; Stevens and Ciesielski 1986; Knox 2003) that is also assumed to be adiabatic and frictionless (Bluestein 1993; Schultz and Schumacher 1999). Thus, the potential vorticity along isentropic surfaces[2] (IPV_g) is often used, where the necessary condition for inertial instability is $IPV_g < 0$. However, as emphasized in Blanchard et al. (1998), the atmosphere does not need to be inertially unstable to be a factor in the spreading of convective outflows aloft. An atmosphere that is preconditioned with weak inertial *stability* may be more susceptible to mesoscale divergent circulations through convective feedbacks (Seman 1994) than an atmosphere with strong inertial stability. Furthermore, if the inertial stability is positive but weak, the restoring forces may be weak enough to result in relatively broad divergent circulations that are hypothesized to encourage convective growth over mesoscale areas. Therefore, it is important to assess the inertial stability of the environment using IPV_g, and not just the geostrophic absolute vorticity,

[2] See Schultz and Schumacher (1999) for a review of methods to diagnose inertial instability on isentropic surfaces or equivalently, dry symmetric stability (Emanuel 1979).

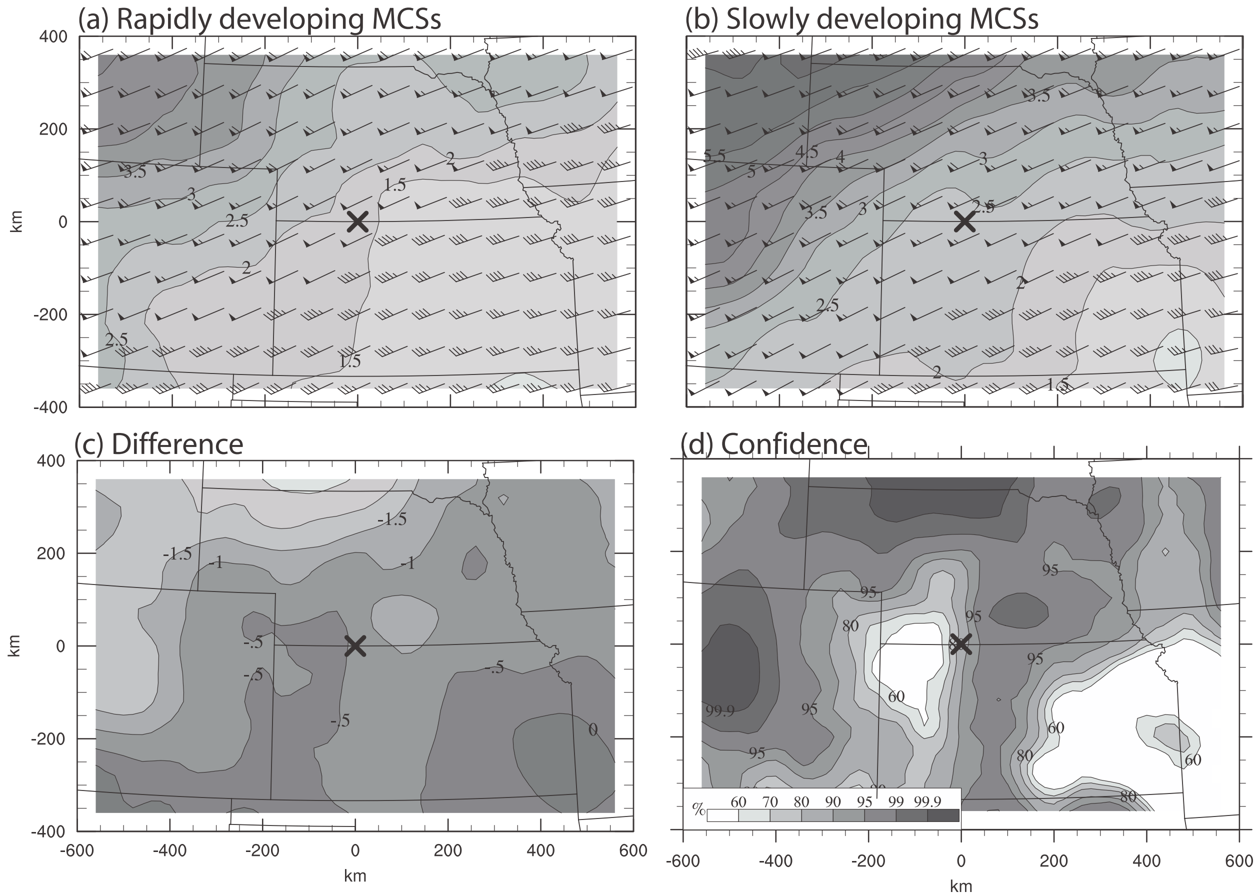

FIG. 10. As in Fig. 6, but a comparison of the geostrophic potential vorticity (in standard potential vorticity units where 1 PVU = 10^{-6} m^2 s^{-1} K kg^{-1}) and wind vectors on the 345-K surface between the RDMs and SDMs. Wind barbs depict the geostrophic wind on the 345-K surface with half (full) barbs representing 2.5 to 7.5 (7.5 to 12.5) kt and pennants starting at 50 kt.

since IPV_g takes the static stability of the atmosphere into account—a condition of weak isentropic inertial stability (i.e., small but positive IPV_g) could be met in regions with very small static stability, regardless of the magnitude of the absolute vorticity.

The RDMs indeed tend to develop in an environment with significantly smaller IPV_g nearby than for the SDMs (Fig. 10) particularly in the area to the east-northeast of the first storms location (centered near $x = 100$ km and $y = 75$ km in Fig. 10d). Furthermore, the confidence is over 99% (and even above 99.9%) over a larger area to the north of the first storms location (centered near $x = -50$ km and $y = 350$ km in Fig. 10d), which is the result of the strong anticyclonic shear on the equatorward side of the enhanced upper-tropospheric geostrophic flow. This suggests that the first storms for the RDMs often take shape in an atmosphere that is noticeably more conducive to the rapid spreading of convective outflows aloft.

Since IPV_g is not a factor that is emphasized much in past studies of MCS environments and, to the authors' knowledge, is not used much in MCS forecasting, we attempt to define ranges of values that could be useful as forecast guidance. Distributions of IPV_g are examined in a region near and ahead of the region where the first storms develop. Although there is a wide range in the maximum and minimum values of IPV_g, the interquartile ranges of IPV_g on the 345-K surface do not overlap (Fig. 11)—75% of the IPV_g values for the rapidly (slowly) developing MCSs are greater than (less than) 1 PVU. This suggests that, given other conditions favorable for rapid upscale growth such as large CAPE (Fig. 7), forecasters might have more confidence in predicting a rapid upscale transition if the upper-level IPV_g on the 345-K isentropic surface (which is usually found between 200 and 250 hPa in these data) becomes smaller than 1 PVU.

3) VERTICAL WIND SHEAR

The vertical shear profile is another important factor to consider in the development of MCSs (Bluestein and Jain 1985; Weisman et al. 1988; Johns 1993; Coniglio

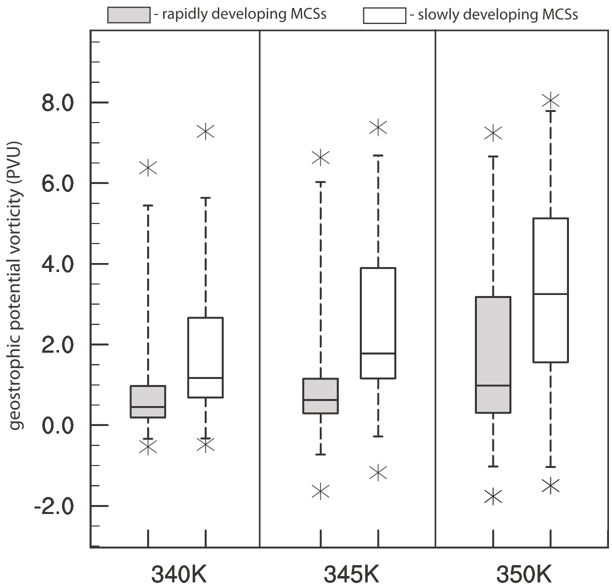

FIG. 11. Box plots representing the distribution of the geostrophic potential vorticity on the 340-, 345-, and 350-K potential temperature surfaces within a 50 km by 50 km box centered on $x = 50$ km and $y = 50$ km in Fig. 10d. The asterisks represent the minimum and maximum of the distributions, the dashed lines extend to the 10th and 90th percentiles, the boxes enclose the 25th and 75th percentiles, and the solid horizontal line in each box represents the median of the distribution. The distributions were calculated using the subsets with a more stringent definition of rapidly and slowly developing MCSs; namely, the 23 MCSs that took ≤4 h to develop were used in the rapidly developing subset and the 27 MCSs that took ≥8 h to develop were used in the slowly developing subset above.

et al. 2006). The low-level (0–3 km) shear[3] (Fig. 12) is slightly larger overall for the RDMs and the differences are statistically significant in a small area downshear of the first storms region (near $x = 200$ km and $y = -50$ km in Fig. 12d). However, a much larger area of significant differences is found in the shear profile above 3 km. For example, the magnitudes of 3–10-km shear are found to be significantly smaller for the RDMs over a much larger area compared to the 0–3-km shear, particularly south of the first storms location and in the downshear direction (Fig. 13d).

A hypothesis for the above result of weaker deep-layer shear for the RDMs is that the weaker deep-layer shear favors multicell thunderstorms over more persistent supercell structures that could delay the development into an MCS (Weisman and Klemp 1982; Rasmussen and Blanchard 1998; Bluestein and Weisman 2000). Upon a subjective inspection of the radar dataset, the first storms exhibit supercell characteristics and/or remain discrete for 25 out of the 39 SDMs (64%), whereas the first storms exhibit supercell characteristics and/or remain discrete for 17 out of the 38 RDMs (45%). Many of the SDMs that do not contain supercell characteristics in their early stages consist of multicells over the high plains within relatively dry low-level environments. This suggests at least some tendency for the SDMs to develop in environments that favor discrete or supercell modes for longer periods. However, what stood out the most was the tendency for the initial storms of the RDMs to be plentiful and develop in a relatively confined region. This is consistent with Dial et al. (2010), who found a more rapid evolution to linear modes along synoptic boundaries when the number of initial storms was larger.

Another possible reason for the smaller 3–10-km shear noted for the RDMs is that the deep and overall stronger shears for the SDMs are delaying the development of a sufficiently strong cold pool capable of organizing the convection (Weisman et al. 1988). Furthermore, numerical simulations of linear convective development suggest that retriggering of convection along a spreading cold pool is favored as more of the total vertical wind shear is confined to low levels (Rotunno et al. 1988; Weisman et al. 1988; Weisman and Rotunno 2004). Although the mean environment for the RDMs still contains a fair amount of 3–10-km shear (Fig. 13a), a vertical shear profile that contains more of the total shear in low levels distinguishes the RDMs from the SDMs (cf. Figs. 12 and 13). However, it is emphasized that a shear profile with a large portion of the line-perpendicular shear confined to low levels is *not* characteristic of the shear profile ahead of long-lived MCSs once they develop, as shown later in section 3c.

c. *Environmental factors in MCS longevity*

To examine environmental factors influencing MCS longevity, a subset of 32 MCSs for which the time difference between the genesis and decay stage ≥8 h [i.e., the long-lived MCSs (LLMs)] is compared to a subset of 30 MCSs for which the time difference between the genesis and decay stage is ≤5 h [i.e., the short-lived MCs (SLMs)]. This comparison addresses the forecast problem of determining how long an MCS will last once genesis has occurred to the extent that the longevity of the MCS can be predicted from the environments ahead of the developing MCS. A few points need to be considered when interpreting the results for the LLM and SLM subsets. Note that the composite analyses presented for these subsets (Figs. 15–22) are mostly confined to a region ahead of the MCS location since it is found that the RUC analyses usually contain a signal from the developing MCS itself (noted particularly in Fig. 18) and this study is focused on the environment that is likely not modified significantly by the existing

[3] The magnitude of the vector difference between the cited levels is referred to as the shear throughout the paper.

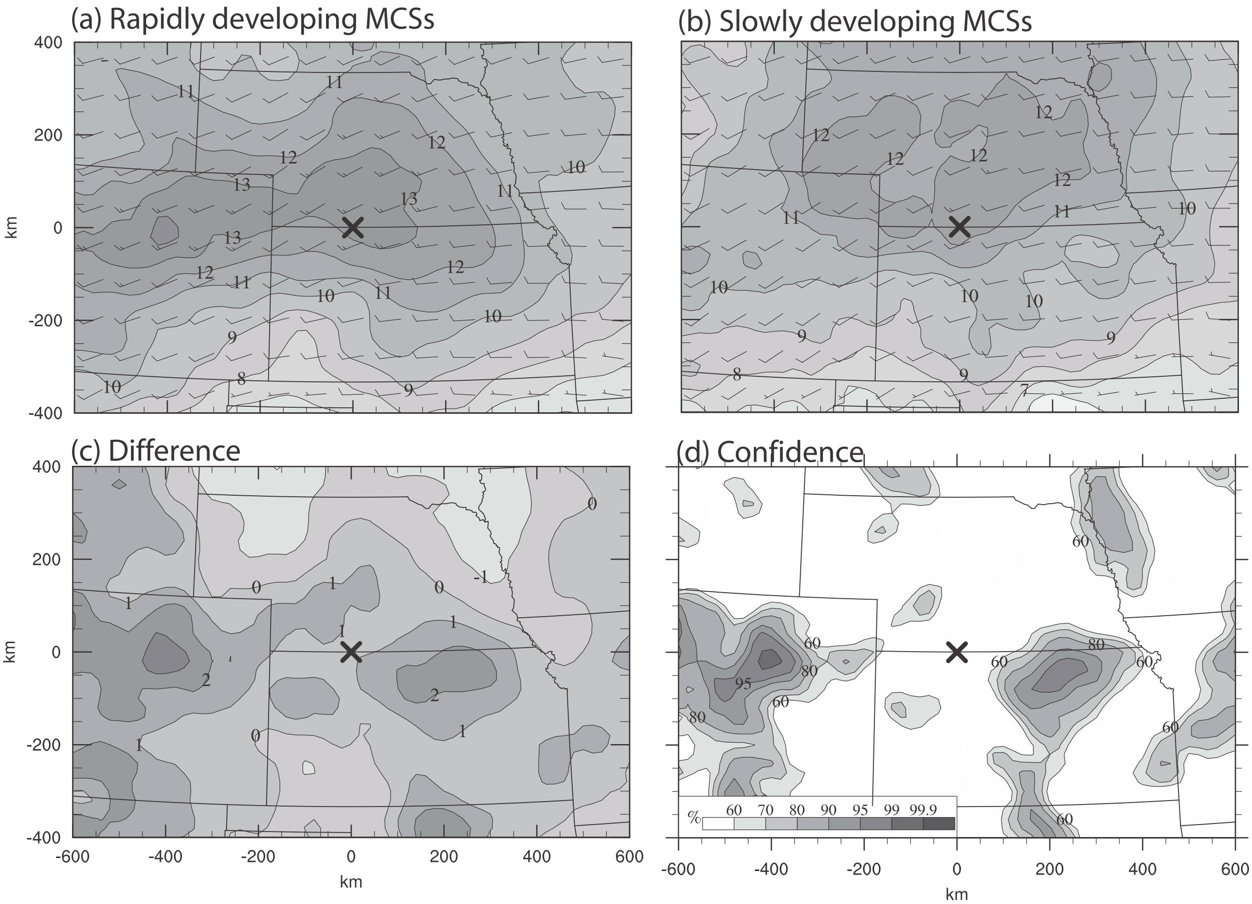

FIG. 12. As in Fig. 6, but a comparison of the 0–3-km wind shear magnitude (m s^{-1}) and 0–3-km wind shear vectors between the RDMs and SDMs. Half (full) barbs represent 2.5–7.5 (7.5–12.5) m s^{-1}.

convection. Furthermore, although the cases are not restricted to nocturnal events, most MCSs in this dataset develop after local sunset or appear to be elevated above a frontal zone. Since the RUC analyses for the comparison of LLMs and SLMs are valid at the time of MCS genesis, which of course is usually later in the day than the time of convective initiation, the composites of the LLM and SLM environments represent nocturnal environments more so than the composites of the RDM and SDM environments.

1) LLJ AND THERMODYNAMIC ENVIRONMENT

It is interesting that the mean LLJ for the SLMs is slightly more veered than the mean LLJ for the LLMs (Fig. 15). This is interesting because the SLMs developed in similar regions, but tended to develop *earlier* in the evening compared to the LLMs (Fig. 14). This shows that the flow configurations for the LLMs tended to favor a LLJ that remained backed for longer periods compared to the flow configuration and LLJ for the SLMs. Furthermore, the composite 500-m AGL flow at the time of MCS genesis shows a mean LLJ that is stronger for the SLMs than the mean LLJ for the LLMs (Fig. 15). This does not, however, indicate that LLJs tended to be stronger overall for the SLMs; rather, it indicates that the LLJ tended to be further along in its inertial oscillation at the time the shorter-lived MCSs develop. This is an interesting finding, but the more statistically significant finding here is that the mean LLJ for the SLMs is confined to a much narrower corridor compared to the LLJ for the LLMs (Fig. 15). This is indicated by the large region of >99.9% confidence to the far east-southeast of the MCS, in which the wind speed is significantly stronger for the LLMs (near $x = 500$ km and $y = -300$ km in Fig. 15d). This suggests that the spatial coverage of the strong southerly flow and its eastward extent is an important feature of long-lived MCS environments. The CAPE is found to be significantly larger for the LLMs in the same region that exhibits the eastward extension of the strong southerly flow (Fig. 16). This suggests a result that was expected, namely that long-lived MCSs are associated with strong southerly inflow of more unstable air over a longer corridor than for short-lived MCSs.

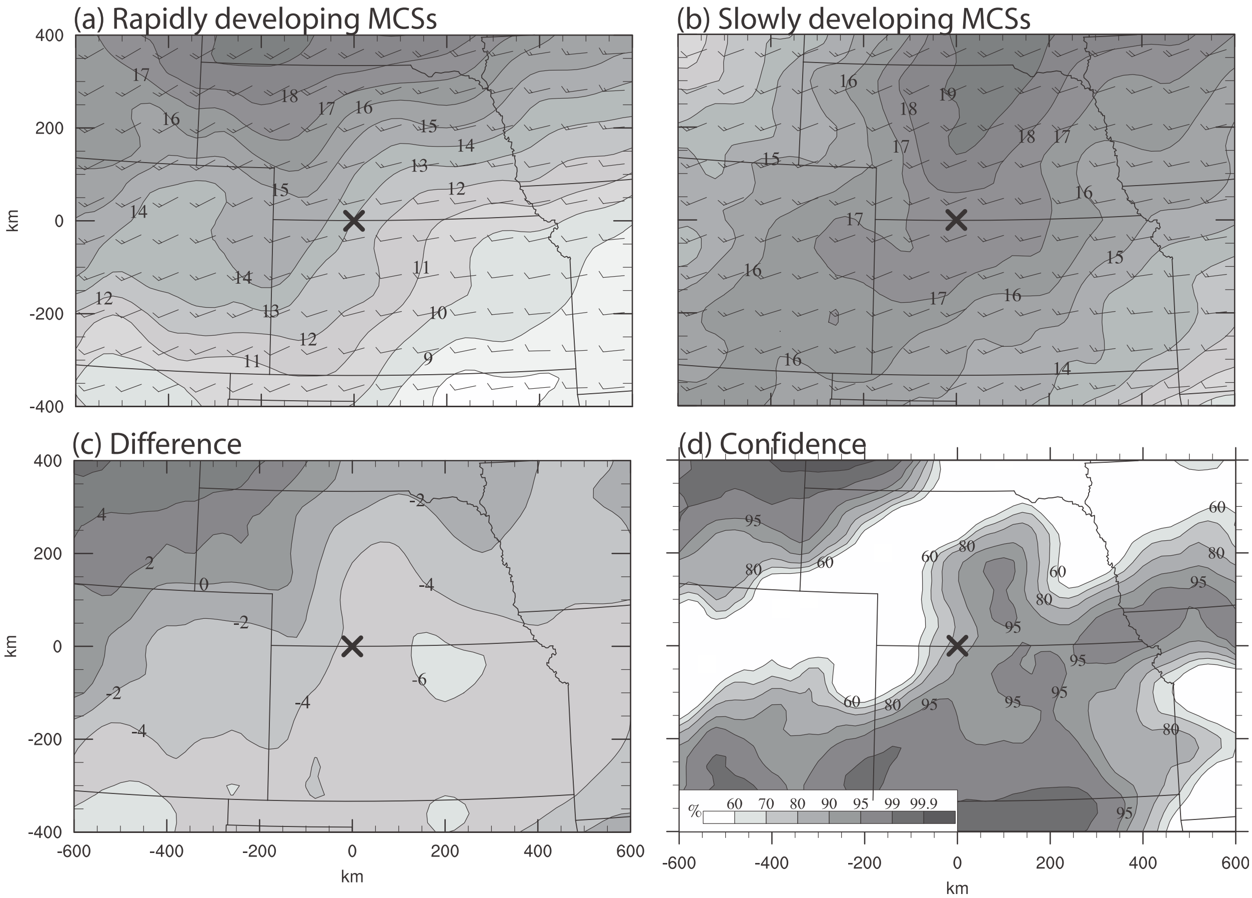

FIG. 13. As in Fig. 6, but a comparison of the 3–10-km wind shear magnitude (m s^{-1}) and 3–10-km wind shear vectors between the RDMs and SDMs. Half (full) barbs represent 2.5–7.5 (7.5–12.5) m s^{-1}.

2) Storm-relative inflow and frontogenesis

A better-defined frontal zone is suggested for the LLMs with stronger MCS-relative easterlies near and ahead of the MCS genesis region at both 10 m and 500 m AGL (Figs. 15–17). This provides a zone of significantly stronger storm-relative inflow and stronger shear (although not significantly so) for the maturing MCSs (especially at 500 m AGL; see Fig. 17). A corridor of larger storm-relative inflow is found near the MCS genesis region for both the LLMs and SLMs, particularly along the northern half of the developing MCS for the LLMs (Figs. 17a,b), which is often located north of the surface frontal boundary. But in comparing the magnitudes between the two subsets, the storm-relative wind speeds are found to be significantly larger for the LLMs (Figs. 17c,d). This is consistent with the hypothesis that strong inflow of the potentially unstable upstream air is an important factor in the fast downwind propagation of MCSs (Evans and Doswell 2001; Gale et al. 2002; Corfidi 2003).

Figures 15 and 16 also bring to light processes associated with frontal zones and LLJs. While it has long been recognized that the LLJ is an efficient moisture transport mechanism (Means 1954; Rasmussen 1967; Helfand and Schubert 1995) and is a source of large-scale destabilization through warm advection (Maddox 1983; Johns and Doswell 1992), the frontogenetical character of the boundary can be important for distinguishing classes of MCSs. Augustine and Caracena (1994) show that relatively large and heavy-rain-producing MCSs occur with a stronger frontogenetical signal at 850 hPa. Trier et al. (2006) argue that long-lived MCSs are aided by the frontogenetical lifting of air by the LLJ, which produces a zone of elevated conditional instability. The results in this study confirm these findings—an elongated corridor of positive frontogenesis is found ahead of the LLM genesis region (from ~y = 100 km to y = 500 km in Fig. 18a) that is not present for the SLMs (Fig. 18b). The surface moisture content and the CAPE of surface-based parcels are not found to be significantly different between the LLMs and SLMs (not

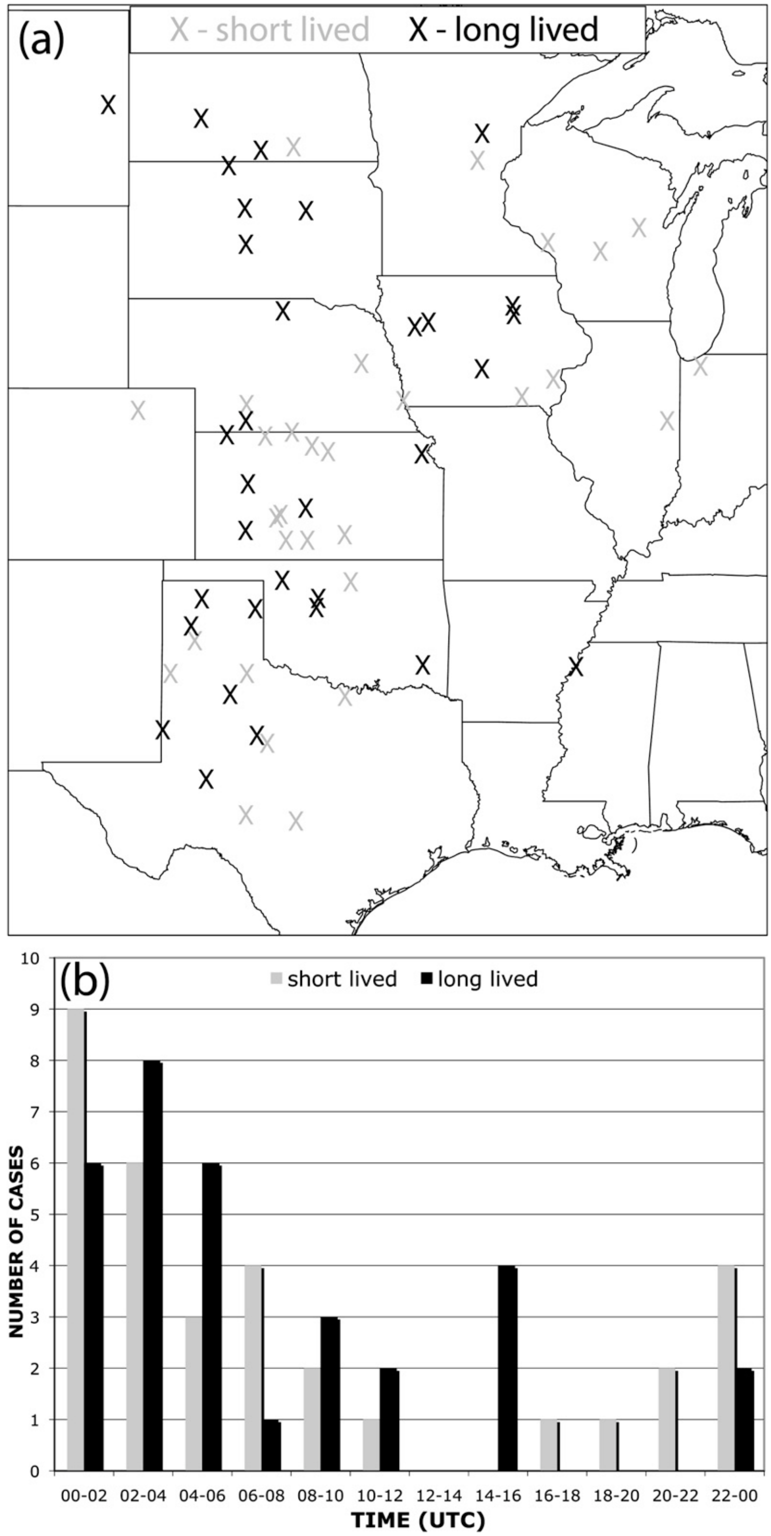

FIG. 14. (a) The location of the MCS genesis for the LLMs (black) and SLMs (gray). (b) Histogram of the time (UTC) of the MCS genesis for the LLMs (black) and SLMs (gray).

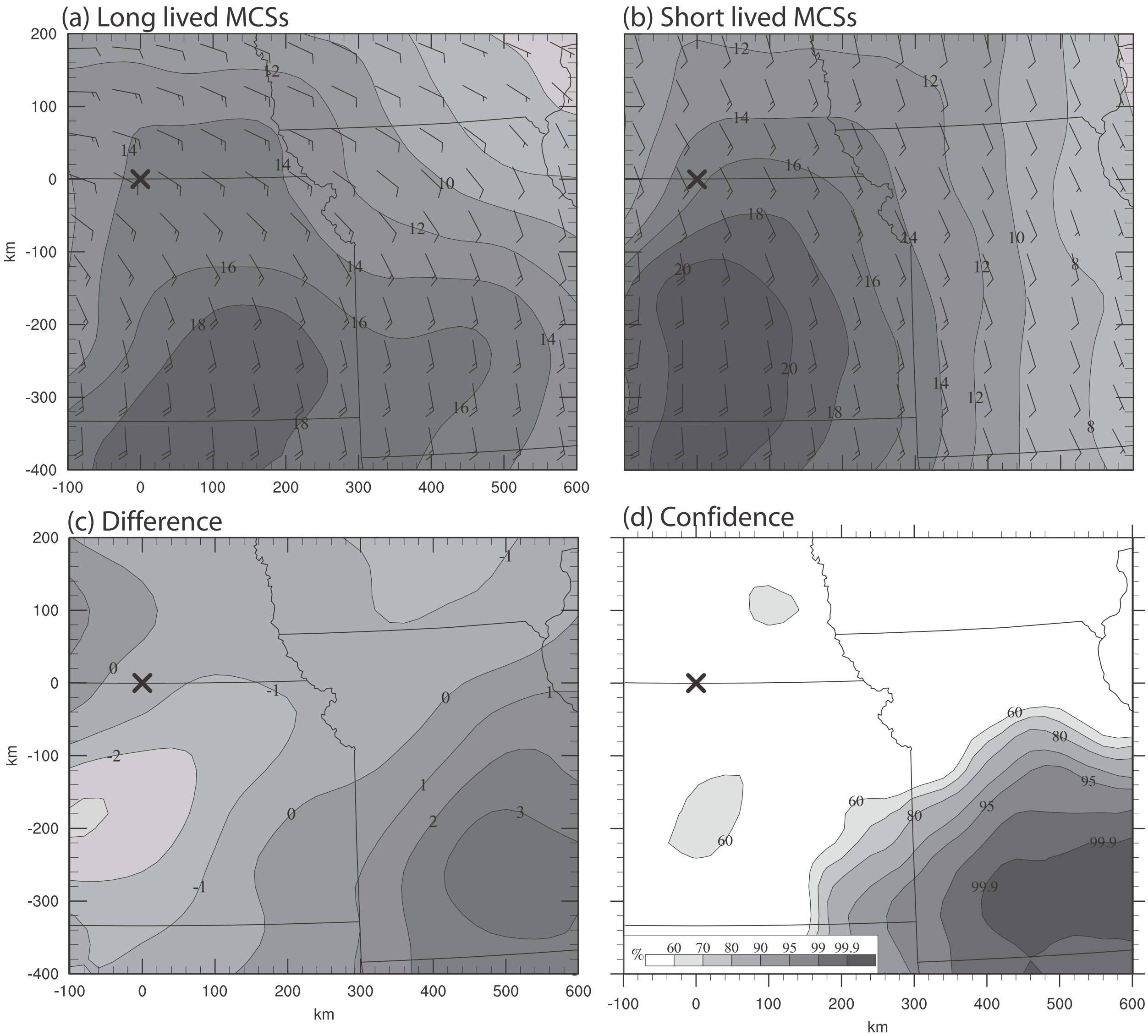

FIG. 15. Contours of the 500-m AGL wind speed (kt) and wind vectors for the (a) 32 long-lived MCSs and (b) the 30 short-lived MCSs. (c) The difference in the mean 500-m AGL wind speed between the long-lived and short-lived MCSs and (d) contours of the confidence that the distributions are different based on the WMW test (see text for details). Barbs denote the 500-m AGL wind vector every 5 kt with half (full) barbs starting at 2.5 (7.5) kt. Note the change in the size and location of the plotting domain compared to the figures comparing the rapidly developing and slowly developing MCSs to focus on the environment ahead of the MCS leading edge, which is denoted by the X.

shown). However, the available moisture, and CAPE of elevated parcels, is found to be significantly larger for the LLMs in an elevated layer in the vicinity of the enhanced frontogenesis (Fig. 19). This is illustrated as a corridor of higher θ_e that extends farther east from the MCS genesis region for the LLMs (Fig. 19a) and represents the "pooling" of deeper moisture along the stronger frontal zone (Johns and Hirt 1987; Tuttle and Davis 2006). It is interesting that the significantly higher mean 800-hPa θ_e values for the LLMs are located near and to the northeast of the enhanced 900-hPa frontogenesis (Figs. 18 and 19). Examination of the θ_e and frontogenesis fields at other pressure levels shows that the axis of significantly higher θ_e shifts to the northeast away from the frontogenesis maximum at 900 hPa as the pressure level decreases and the differences in θ_e between the two subsets are no longer significant in the vicinity of the MCS at 700 hPa. This suggests that the mesoscale vertical circulation associated with the frontogenesis is often responsible for the higher elevated θ_e and is a factor in MCS longevity, as suggested in Trier et al. (2006).

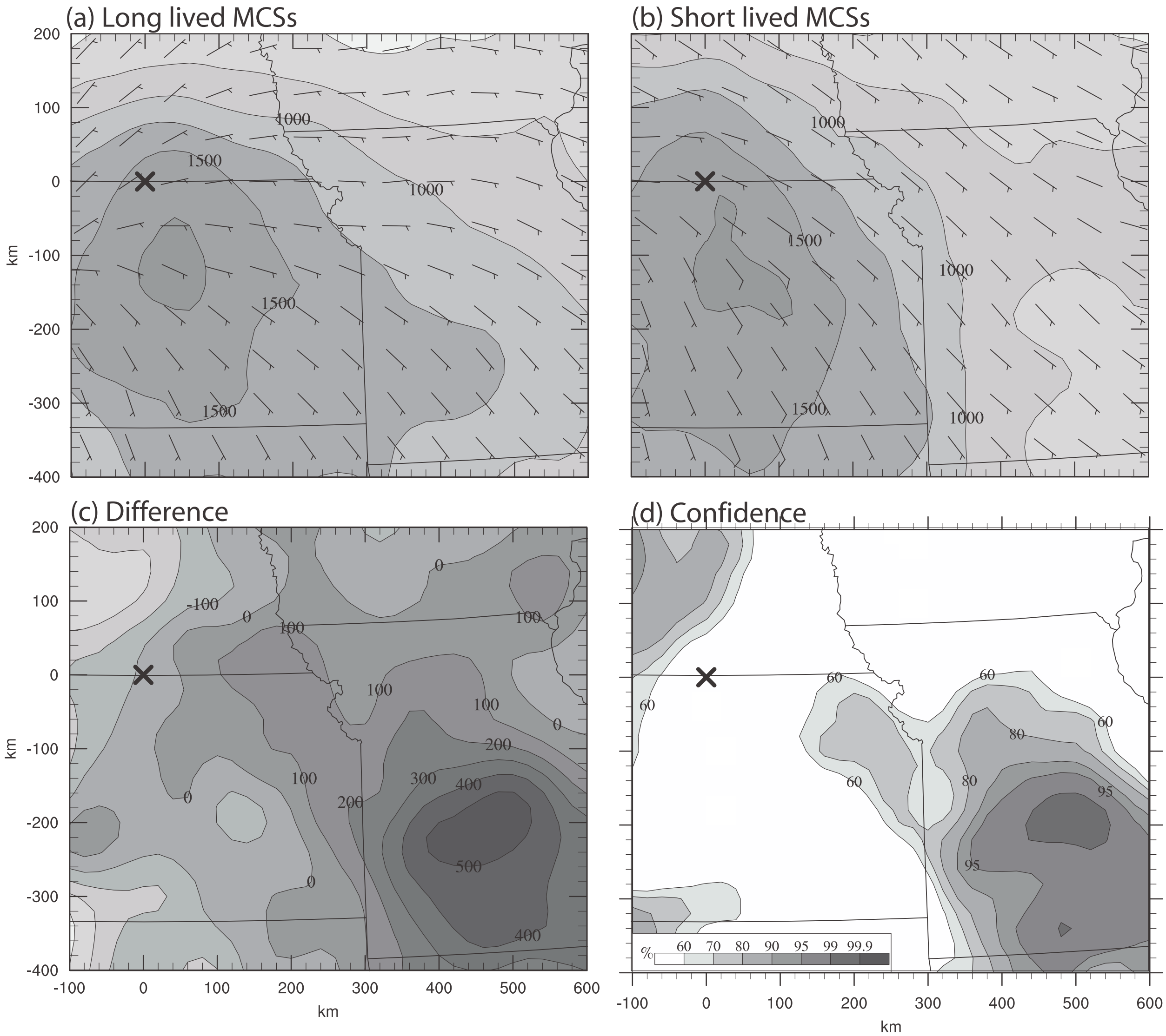

FIG. 16. As in Fig. 15, but a comparison of mean CAPE (J kg^{-1}) and 10-m wind vectors between the LLMs and SLMs. A hybrid most-unstable–mixed parcel is used to calculate the CAPE as follows: at every 50 hPa in the vertical, the CAPE is calculated using a parcel with a wet-bulb potential temperature that results from averaging the temperature and water vapor mixing ratio over the neighboring 100-hPa layer. The resulting CAPE in the figure is the maximum of those calculations.

3) VERTICAL WIND SHEAR

Finally, we return to the analysis of the vertical shear profile. Recall that the RDMs have significantly larger 0–3-km shear in a relatively small region ahead of the first storms (Fig. 12d), but more significant differences are found in the shear above 3 km, in which the magnitudes are significantly less for the RDMs (Fig. 13d). For the LLM and SLM subsets, most of the MCSs are captured at a stage after the surface layer decouples from the free atmosphere above or when much of the MCS is elevated above a frontal zone. Therefore, the composites for the LLM and SLM subsets represent more of a nocturnal environment than the composites for the RDM and SDM subsets. Given the frequency of nocturnal environments in the LLM and SLM subsets, the level over which to characterize the low-level shear is not clear—it may not be appropriate to use the 10-m wind as the lower bound in the shear calculations if the 10-m wind is not often part of the effective inflow layer (James et al. 2005; Thompson et al. 2007). For this reason, the shear over multiple layers in the lower troposphere is examined in detail for the LLM and SLM subsets. It is found that the shear in layers below 3 km AGL, whether the lower bound is taken to be 10 m, 500 m, or 1 km AGL, is generally not found to be

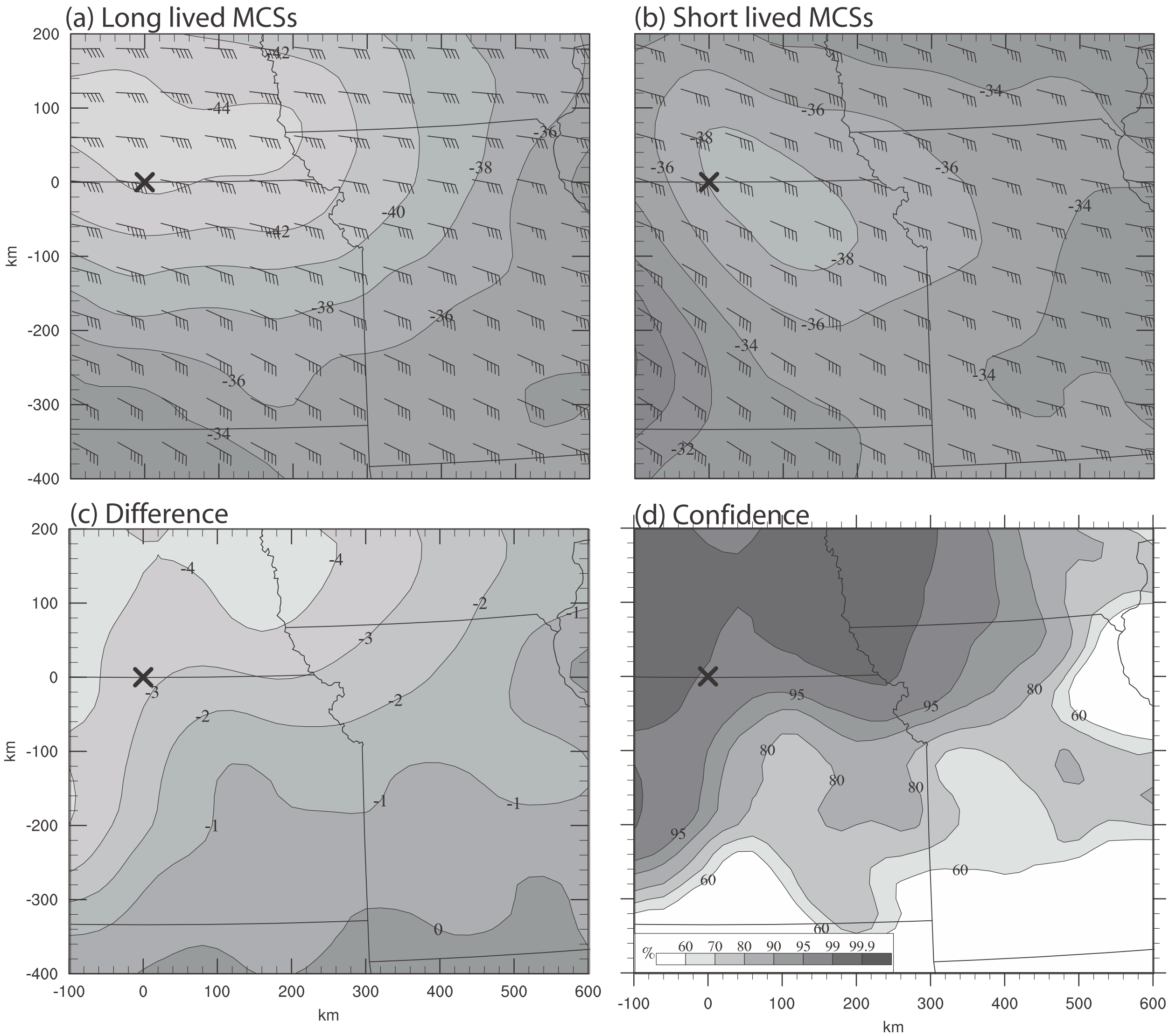

FIG. 17. As in Fig. 15, but a comparison of the component of MCS-relative wind parallel to the MCS motion (kt) at 500 m AGL between the LLMs and SLMs. Wind barbs denote the MCS-relative 500-m AGL total wind vector every 5 kt with half (full) barbs starting at 2.5 (7.5) kt.

significantly different between the LLMs and SLMs out to 300 km along the ensuing path of the system. Out of all the low-level layers examined, only the shear in the 0.5–2-km layer exhibits some areas with significant differences (>95%) in the 300 km ahead of the ensuing MCS (Fig. 20). The enhanced frontal zone and significantly larger storm-relative inflow at 500 m AGL (Fig. 17) is consistent with a zone of enhanced 0.5–2-km shear ahead of the maturing LLMs (Fig. 20a), but the values of 0.5–2-km shear in this region for the LLMs are not significantly different than the values of 0.5–2-km shear for the SLMs until about 200 km ahead of the MCS location (Fig. 19d). In fact, none of the shear values over the 0–1-, 0–2-, 0–3-, 0.5–3-, or 1–3-km AGL layers was found to be significantly different between the LLMs and SLMs anywhere near the undisturbed MCS genesis region. This result questions the utility of the shear magnitudes in low levels to distinguish between long-lived and short-lived MCSs in a forecast application.

However, values of mid- to upper-level tropospheric shear, in layers with the lower bound somewhere above 2–3 km AGL, are found to be significantly larger for the LLMs (Fig. 21). For example, the 2–6-km shear is much larger for the LLMs in a large region ahead of the MCS genesis, with significance values >95% and some grid points showing a significance of >99% (Fig. 21d). As a consequence, the shear over the 0.5–6-km layer is significantly larger ahead of the LLMs (Fig. 22), with mean values between 18 and 22 m s^{-1}. It is generally recognized that a moderate amount of shear over the

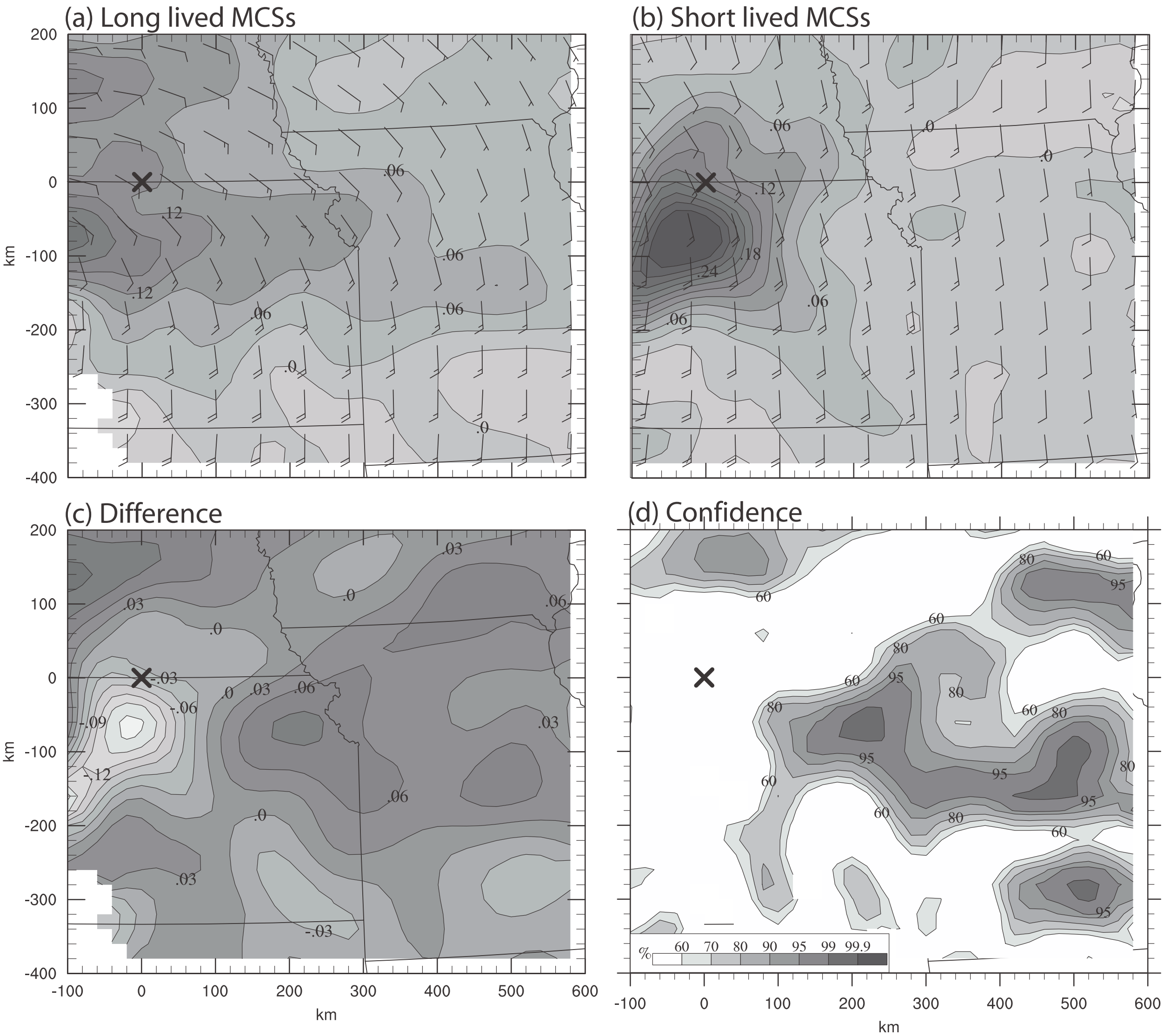

FIG. 18. As in Fig. 15, but a comparison between the mean 2D frontogenesis (K km^{-1} h^{-1}) and winds (kt) at 900 hPa between the LLMs and SLMs. Barbs denote the 900-hPa wind every 5 kt with half (full) barbs starting at 2.5 (7.5) kt.

lowest 6 km or so, like that found in this study (Fig. 22), is important for organized severe convection (Weisman and Klemp 1982; Rasmussen and Blanchard 1998). However, the significantly larger deep-layer shear found for the LLMs is primarily the result of the shear that is elevated above the surface (above 2–3 km AGL) and has a smaller contribution from the low-level shear. This contrasts the findings of the comparison between rapidly and slowly developing MCSs, in which the shear in the lowest 3 km was mainly responsible for the larger deep-layer shear. Combined with this difference in the shear profiles found between the RDMs and SDMs, *this suggests that the optimal depth over which to examine the shear magnitude in the forecasting of MCSs changes from low levels prior to the development of the MCS to mid levels once the MCS has developed*. The shift in attention to the shear profile above the surface is likely most important for nocturnal MCSs, in which long-lived MCSs can tap into the efficient inflow of high θ_e air well above the surface (Fig. 19). The shear in this elevated layer can help maintain the convective updrafts along the leading edge of the cold pool or whatever mechanism may be forcing the continued generation of convection (Shapiro 1992; Fovell and Dailey 1995; Moncrieff and Liu 1999; Coniglio et al. 2006).

4. Summary and discussion

Hourly RUC analyses from 94 MCSs that develop a well-defined leading convective line were used to examine the mesoscale features of MCS environments. A

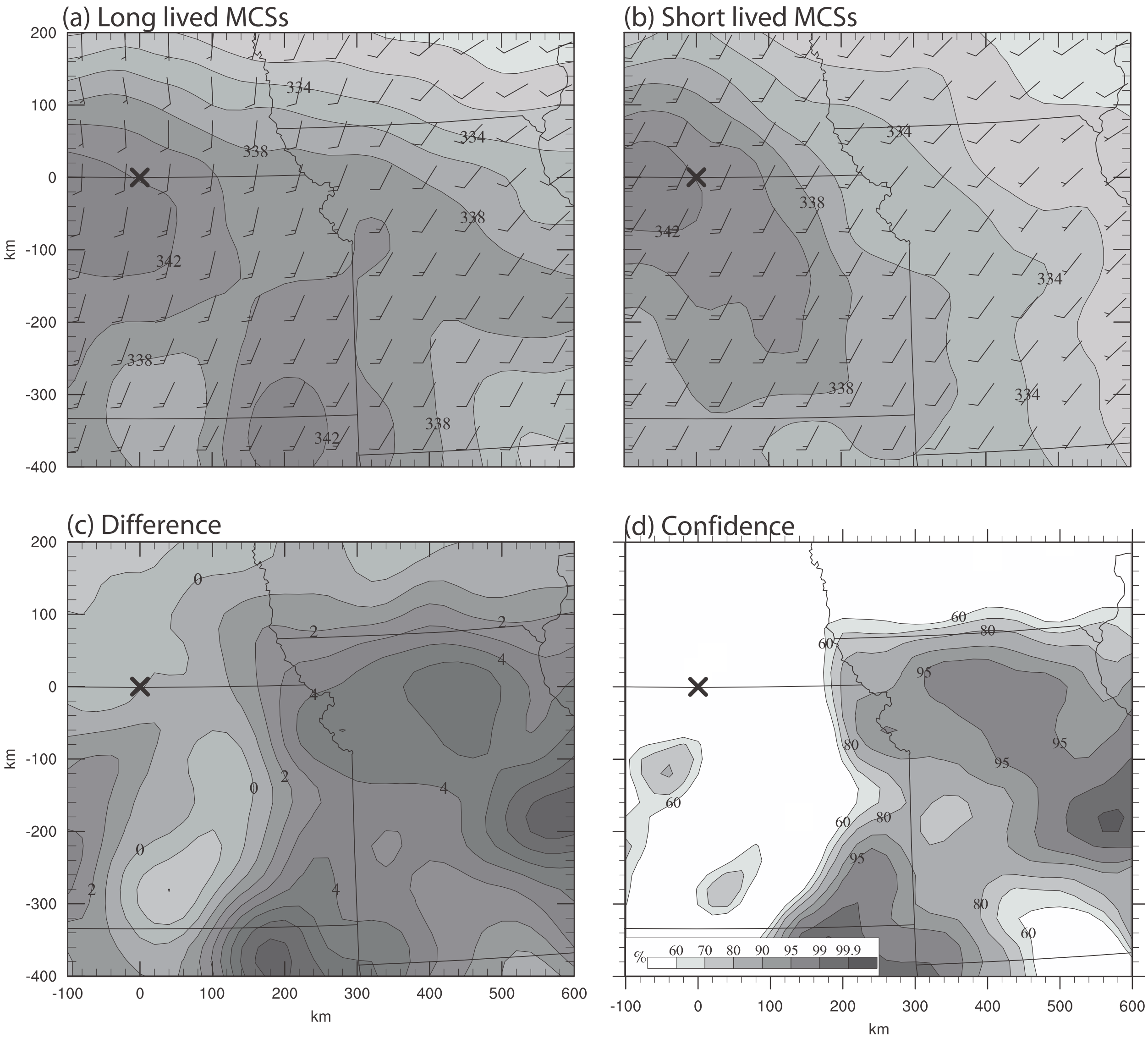

FIG. 19. As in Fig. 15, but a comparison of the 800-hPa equivalent potential temperature (K) and 800-hPa winds (kt) between the LLMs and SLMs. Barbs denote the 800-hPa wind every 5 kt with half (full) barbs starting at 2.5 (7.5) kt.

primary goal is to distinguish the environments of MCSs that develop rapidly from those that develop slowly and to distinguish the environments of long-lived and short-lived MCSs. Knowledge of these environments could have implications for the prediction of the type of severe weather produced by a convective episode and the duration of the severe weather produced. The RUC analyses are chosen for this study since they are frequently used by forecasters as proxies to operational radiosonde observations when assessing the three-dimensional characteristics of the preconvective and near-storm environment.

Composite analyses of all 94 MCSs capture the synoptic-scale features known to be associated with MCS development, including broad midlevel cyclonic vorticity advection, an upper-tropospheric wind maximum poleward of the MCS first storms, lower-tropospheric warm advection enhanced by a frontal zone, and an impinging low-level wind maximum. The composite analyses also capture the mesoscale inertial oscillation of the nocturnal LLJ and suggest that the change in sign of the component of the ageostrophic wind parallel to MCS motion from negative to positive, and the associated loss of storm-relative inflow and convergence, is associated with MCS decay and not necessarily a weakening of the overall intensity of the LLJ.

A comparison of the mean composites of the preconvective environments prior to the development of the first

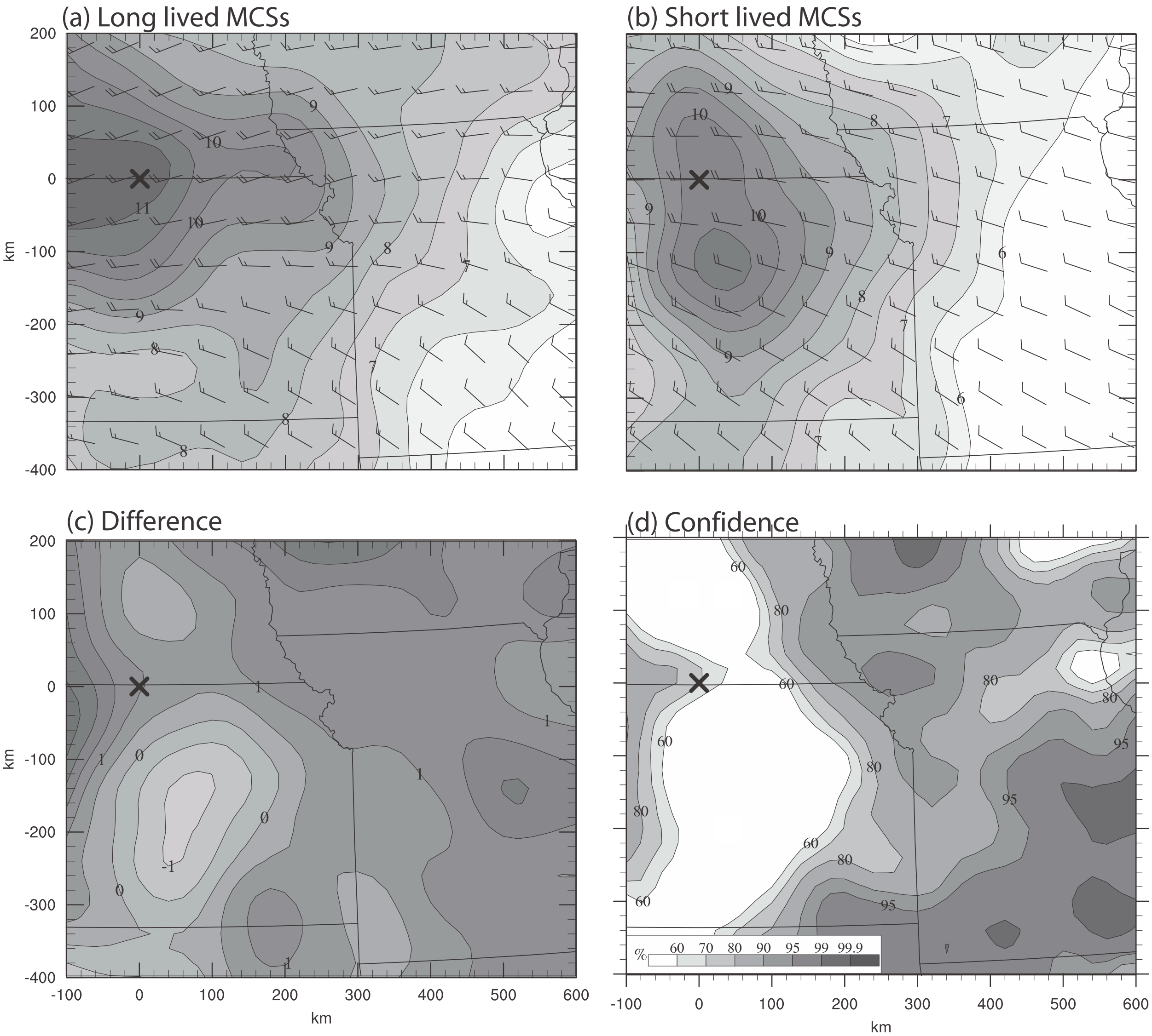

FIG. 20. As in Fig. 15, but a comparison of the 0.5–2-km vertical wind shear magnitude (m s^{-1}) and 0.5–2-km wind shear vectors between the LLMs and SLMs. Half (full) barbs represent 2.5–7.5 (7.5–12.5) m s^{-1}.

storms reveals several statistically significant differences among the rapidly developing MCSs (RDMs) and slowly developing MCSs (SDMs), including the following:

- a stronger LLJ located closer to the first storms region for the RDMs;
- much larger CAPE, DCAPE, and potential instability ($\partial\theta_e/\partial z < 0$) for the RDMs, despite smaller low- to midlevel lapse rates;
- smaller 3–10-km vertical wind shear for the RDMs; and
- smaller geostrophic potential vorticity along isentropic surfaces (IPV_g) for the RDMs.

Although the strong inflow of higher CAPE air is likely of primary importance in the speed at which MCSs develop, the larger potential instability could encourage more slabular lifting and a more rapid "filling in" of strong convection along the cold pool, and hence a more rapid transition to an MCS. Furthermore, there was evidence that the weaker shear above 3 km allowed for more persistent supercell or discrete modes for the convection that preceded the SDMs. But the weaker shear above 3 km also could indicate an environment that supports more efficient retriggering of convection along the spreading cold pool (Weisman et al. 1988).

Although negative IPV_g (and absolute vorticity), and associated inertial instability, has been deemed a factor in MCS development because it can facilitate strong outflows aloft (Seman 1994; Blanchard et al.

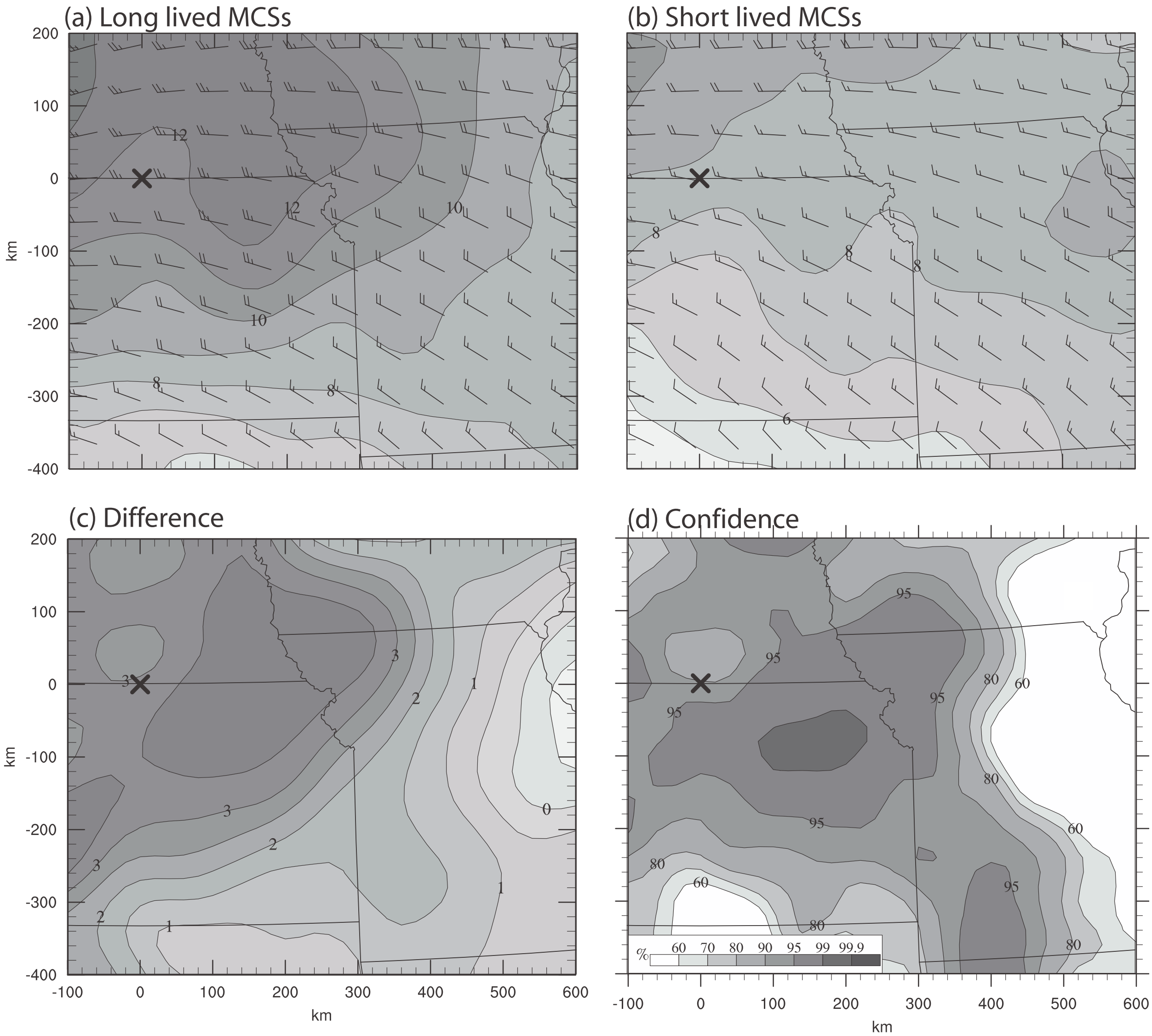

FIG. 21. As in Fig. 15, but a comparison of the 2–6-km vertical wind shear magnitude (m s^{-1}) and 2–6-km wind shear vectors between the LLMs and SLMs. Half (full) barbs represent 2.5–7.5 (7.5–12.5) m s^{-1}.

1998), small IPV$_g$ has not been emphasized in past literature as a variable to consider in forecasting the speed of the transition to an MCS. Again, the results suggest a primary role of CAPE and potential instability, but they also suggest that small (or negative) IPV$_g$ could be a factor that needs to be considered in the determination of the speed at which an MCS may develop from a cluster of convective cells. The results suggest that *rapidly developing MCSs (those that develop in 4–5 h) become increasingly more likely if the upper-level* IPV$_g$ < 1 PVU *in the preconvective environment*.

A comparison of the mean composites of the environments ahead of the genesis of long-lived MCSs (LLMs) and short-lived MCSs (SLMs) reveal several statistically significant differences, including the following:

- a much broader southerly low-level wind maximum for the LLMs, despite a stronger mean LLJ at the time of MCS genesis for the SLMs;
- a more well-defined frontal zone and stronger storm-relative low-level easterlies near and north of the MCS genesis region for the LLMs;
- stronger mean low-level frontogenesis for the LLMs and an associated region of higher θ_e in the lower troposphere elevated above the surface; and
- stronger deep-layer (0.5–6 km AGL) vertical wind shear for the LLMs, in which *the differences in shear*

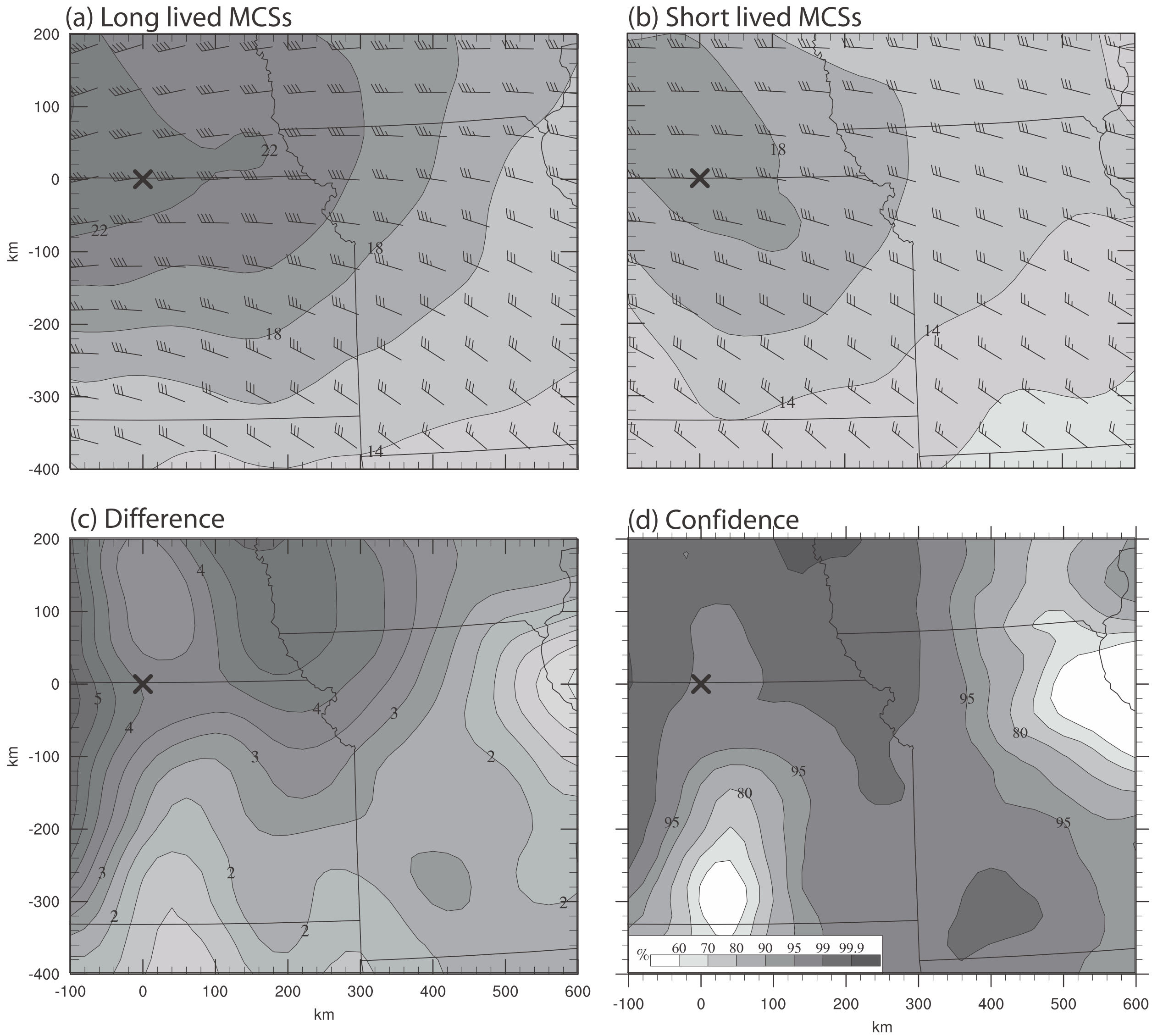

FIG. 22. As in Fig. 15, but a comparison of the 0.5–6-km vertical wind shear magnitude (m s^{-1}) and 0.5–6-km wind shear vectors between the LLMs and SLMs. Half (full) barbs represent 2.5–7.5 (7.5–12.5) m s^{-1}.

in the 2–6-km layer are contributing most to the differences.

It is emphasized that *the shear above 2 km was significantly larger over a wide area* for the LLMs compared to the SLMs, despite few significant differences in the low-level shear ahead of the MCSs. This is consistent with the idea that shear elevated above the ground is important for maintain convection along the cold pool (Coniglio et al. 2006) that feeds on the elevated unstable air after dark found in this study and emphasized in Trier et al. (2006). It also suggests that *the optimal depth over which to examine the shear magnitude in the forecasting of MCSs changes from low levels prior to the development of the MCS to midlevels once the MCS has developed*.

Finally, it is recognized that care must be taken to generate composite analyses so that their interpretation can be meaningful. Although several methods for grouping analyses by characteristic spatial patterns exist and have been applied to meteorological variables (Wallace et al. 1992; Cannon et al. 2002; Coniglio et al. 2004), the dataset employed herein was small enough to allow a subjective determination of the flow features to ensure that prominent features found in the mean analyses are meteorological and not artifacts of the compositing procedure. Much of the general similarity in the background synoptic-scale flow was dictated by the restriction of the MCS dataset to the more robust warm-season-type events and the fact that most of the MCSs developed after dark or above low-level frontal zones. Furthermore, this study is focused more on the ingredients derived from the background environment (e.g., CAPE, vertical wind shear, etc.) than on the particular flow pattern associated with the MCS, which lessens the importance of the procedure used to perform the compositing. Although the results presented herein are not applicable to all situations that produce MCSs, it is believed that the resulting differences in the mean analyses represent robust signals for MCSs that can be identified easily in 20-km RUC analyses, especially for nocturnal MCSs or those that occur above frontal zones. Looking for these signals in short-term forecasts may aid in the difficult problem of forecasting the mesoscale details of strong, propagating MCSs in the warm season.

Acknowledgments. Partial funding was provided by NOAA/Office of Oceanic and Atmospheric Research under NOAA–University of Oklahoma Cooperative Agreement NA17RJ1227, U.S. Department of Commerce. The authors thank the efforts of the NOAA Hollings scholarship program, which supported the second author (JYH) during this project. We also thank Dr. Kim Elmore of the University of Oklahoma–NOAA/Cooperative Institute for Mesoscale Meteorological Studies and Greg Dial and Steve Corfidi of the NOAA/Storm Prediction Center for valuable discussions. Finally, we are thankful to Drs. Matt Parker and Morris Weisman for their very constructive and careful reviews.

REFERENCES

Anderson, C. J., and R. W. Arritt, 1998: Mesoscale convective complexes and persistent elongated convective systems over the United States during 1992 and 1993. *Mon. Wea. Rev.,* **126,** 578–599.

Ashley, W. S., and T. L. Mote, 2005: Derecho hazards in the United States. *Bull. Amer. Meteor. Soc.,* **86,** 1577–1592.

Atkins, N. T., and R. M. Wakimoto, 1991: Wet microburst activity over the southeastern United States: Implications for forecasting. *Wea. Forecasting,* **6,** 470–482.

Augustine, J. A., and F. Caracena, 1994: Lower-tropospheric precursors to nocturnal MCS development over the central United States. *Wea. Forecasting,* **9,** 116–135.

Benjamin, S. G., and Coauthors, 2004: An hourly assimilation-forecast cycle: The RUC. *Mon. Wea. Rev.,* **132,** 495–518.

Bennetts, D. A., and B. J. Hoskins, 1979: Conditional symmetric instability—A possible explanation for frontal rainbands. *Quart. J. Roy. Meteor. Soc.,* **105,** 945–962.

Blackadar, A. K., 1957: Boundary layer wind maxima and their significance for the growth of nocturnal inversions. *Bull. Amer. Meteor. Soc.,* **38,** 283–290.

Blanchard, D. O., W. R. Cotton, and J. M. Brown, 1998: Mesoscale circulation growth under conditions of weak inertial instability. *Mon. Wea. Rev.,* **126,** 118–140.

Bluestein, H. B., 1993: *Synoptic-Dynamic Meteorology in Midlatitudes*. Vol. II. Oxford University Press, 348–350.

——, and M. H. Jain, 1985: Formation of mesoscale lines of precipitation: Severe squall lines in Oklahoma during the spring. *J. Atmos. Sci.,* **42,** 1711–1732.

——, and M. L. Weisman, 2000: The interaction of numerically simulated supercells initiated along lines. *Mon. Wea. Rev.,* **128,** 3128–3149.

Bonner, W. D., 1968: Climatology of the low-level jet. *Mon. Wea. Rev.,* **96,** 833–850.

Bryan, G. H., and J. M. Fritsch, 2000: Moist absolute instability: The sixth static stability state. *Bull. Amer. Meteor. Soc.,* **81,** 1207–1230.

Cannon, A. J., P. H. Whitfield, and E. R. Lord, 2002: Synoptic map-pattern classification using recursive partitioning and principal component analysis. *Mon. Wea. Rev.,* **130,** 1187–1206.

Cohen, A. E., M. C. Coniglio, S. F. Corfidi, and S. J. Corfidi, 2007: Discrimination of mesoscale convective system environments using sounding observations. *Wea. Forecasting,* **22,** 1045–1062.

Coniglio, M. C., D. J. Stensrud, and M. B. Richman, 2004: An observational study of derecho-producing convective systems. *Wea. Forecasting,* **19,** 320–337.

——, ——, and L. J. Wicker, 2006: Effects of upper-level shear on the structure and maintenance of strong quasi-linear mesoscale convective systems. *J. Atmos. Sci.,* **63,** 1231–1252.

——, H. E. Brooks, S. J. Weiss, and S. F. Corfidi, 2007: Forecasting the maintenance of quasi-linear mesoscale convective systems. *Wea. Forecasting,* **22,** 556–570.

Corfidi, S. F., 2003: Cold pools and MCS propagation: Forecasting the motion of downwind-developing MCSs. *Wea. Forecasting,* **18,** 997–1017.

——, S. J. Corfidi, D. A. Imy, and A. L. Logan, 2006: A preliminary study of severe-wind-producing MCSs in environments of limited moisture. *Wea. Forecasting,* **21,** 715–734.

Cotton, W. R., M.-S. Lin, R. L. McAnelly, and C. J. Tremback, 1989: A composite model of mesoscale convective complexes. *Mon. Wea. Rev.,* **117,** 765–783.

Dial, G. L., J. P. Racy, and R. L. Thompson, 2010: Short-term convective mode evolution along synoptic boundaries. *Wea. Forecasting,* in press.

Emanuel, K. A., 1979: Inertial instability and mesoscale convective systems. Part I: Linear theory of inertial instability in rotating viscous fluids. *J. Atmos. Sci.,* **36,** 2425–2449.

Engerer, N. A., D. J. Stensrud, and M. C. Coniglio, 2008: Surface characteristics of observed cold pools. *Mon. Wea. Rev.,* **136,** 4839–4849.

Evans, J. S., and C. A. Doswell III, 2001: Examination of derecho environments using proximity soundings. *Wea. Forecasting,* **16,** 329–342.

Fovell, R. G., and P. S. Dailey, 1995: The temporal behavior of numerically simulated multicell-type storms. Part I: Modes of behavior. *J. Atmos. Sci.,* **52,** 2073–2095.

Fritsch, J. M., R. J. Kane, and C. R. Chelius, 1986: The contribution of mesoscale convective weather systems to the warm season precipitation in the United States. *J. Climate Appl. Meteor.,* **25,** 1333–1345.

Gale, J. J., W. A. Gallus Jr., and K. A. Jungbluth, 2002: Toward improved prediction of mesoscale convective system dissipation. *Wea. Forecasting,* **17,** 856–872.

Gallus, W. A., N. A. Snook, and E. V. Johnson, 2008: Spring and summer severe weather reports over the Midwest as a function of convective mode: A preliminary study. *Wea. Forecasting,* **23,** 101–113.

Hane, C. E., J. A. Haynes, D. L. Andra Jr., and F. H. Carr, 2008: The evolution of morning convective systems over the U.S. Great Plains during the warm season. Part II: A climatology and the influence of environmental factors. *Mon. Wea. Rev.,* **136,** 929–944.

Helfand, H. M., and S. D. Schubert, 1995: Climatology of the simulated Great Plains low-level jet and its contribution to the continental moisture budget of the United States. *J. Climate,* **8,** 784–806.

Hilgendorf, E. R., and R. H. Johnson, 1998: A study of the evolution of mesoscale convective systems using WSR-88D data. *Wea. Forecasting,* **13,** 437–452.

Houze, R. A., Jr., S. A. Rutledge, M. I. Biggerstaff, and B. F. Smull, 1989: Interpretation of Doppler weather radar displays of midlatitude mesoscale convective systems. *Bull. Amer. Meteor. Soc.,* **70,** 608–619.

James, R. P., J. M. Fritsch, and P. M. Markowski, 2005: Environmental distinctions between cellular and slabular convective lines. *Mon. Wea. Rev.,* **133,** 2669–2691.

Jirak, I. L., and W. R. Cotton, 2003: Satellite and radar survey of mesoscale convective system development. *Mon. Wea. Rev.,* **131,** 2428–2449.

——, and ——, 2007: Observational analysis of the predictability of mesoscale convective systems. *Wea. Forecasting,* **22,** 813–838.

Johns, R. H., 1984: A synoptic climatology of northwest-flow severe weather outbreaks. Part II: Meteorological parameters and synoptic patterns. *Mon. Wea. Rev.,* **112,** 449–464.

——, 1993: Meteorological conditions associated with bow echo development in convective storms. *Wea. Forecasting,* **8,** 294–299.

——, and W. D. Hirt, 1987: Derechos: Widespread convectively induced windstorms. *Wea. Forecasting,* **2,** 32–49.

——, and C. A. Doswell III, 1992: Severe local storms forecasting. *Wea. Forecasting,* **7,** 588–612.

Knox, J. A., 2003: Inertial instability. *Encyclopedia of the Atmospheric Sciences,* J. Holton, J. Pyle, and J. Curry, Eds., Academic Press, 1004–1013.

Lanicci, J. M., and T. T. Warner, 1991: A synoptic climatology of the elevated mixed-layer inversion overt he southern Great Plains in spring. Part I: Structure, dynamics, and seasonal evolution. *Wea. Forecasting,* **6,** 181–197.

Maddox, R. A., 1983: Large-scale conditions associated with midlatitude, mesoscale convective complexes. *Mon. Wea. Rev.,* **111,** 1475–1493.

——, C. F. Chappell, and L. R. Hoxit, 1979: Synoptic and meso-α-scale aspects of flash flood events. *Bull. Amer. Meteor. Soc.,* **60,** 115–123.

McAnelly, R. L., J. E. Nachamkin, W. R. Cotton, and M. E. Nicholls, 1997: Upscale evolution of MCSs: Doppler radar analysis and analytical investigation. *Mon. Wea. Rev.,* **125,** 1083–1110.

McNider, R. T., and R. A. Pielke, 1981: Diurnal boundary-layer development over sloping terrain. *J. Atmos. Sci.,* **38,** 2198–2212.

Means, L. L., 1954: A study of the mean southerly wind-maximum in low levels associated with a period of summer precipitation in the middle west. *Bull. Amer. Meteor. Soc.,* **35,** 166–170.

Moncrieff, M. W., and C. Liu, 1999: Convection initiation by density currents: Role of convergence, shear, and dynamical organization. *Mon. Wea. Rev.,* **127,** 2455–2464.

Moore, J. T., F. H. Glass, C. E. Graves, S. M. Rochette, and M. J. Singer, 2003: The environment of warm-season elevated thunderstorms associated with heavy rainfall over the central United States. *Wea. Forecasting,* **18,** 861–878.

Parker, M. D., and R. H. Johnson, 2000: Organizational modes of midlatitude mesoscale convective systems. *Mon. Wea. Rev.,* **128,** 3413–3436.

Proctor, F. H., 1989: Numerical simulation of an isolated microburst. Part II: Sensitivity experiments. *J. Atmos. Sci.,* **46,** 2143–2165.

Rasmussen, E. M., 1967: Atmospheric water vapor transport and the water balance of North America. Part I: Characteristics of the water vapor flux field. *Mon. Wea. Rev.,* **95,** 403–426.

Rasmussen, E. N., and D. O. Blanchard, 1998: A baseline climatology of sounding-derived supercell and tornado forecast parameters. *Wea. Forecasting,* **13,** 1148–1164.

Rotunno, R., J. B. Klemp, and M. L. Weisman, 1988: A theory for strong, long-lived squall lines. *J. Atmos. Sci.,* **45,** 463–485.

Schumacher, R. S., and R. H. Johnson, 2005: Organization and environmental properties of extreme-rain-producing mesoscale convective systems. *Mon. Wea. Rev.,* **133,** 961–976.

——, and ——, 2009: Quasi-stationary, extreme-rain-producing convective systems associated with midlevel cyclonic circulations. *Wea. Forecasting,* **24,** 555–574.

Schultz, D. M., and P. N. Schumacher, 1999: The use and misuse of conditional symmetric instability. *Mon. Wea. Rev.,* **127,** 2709–2732.

Seman, C. J., 1994: A numerical study of nonlinear nonhydrostatic conditional symmetric instability in a convectively unstable atmosphere. *J. Atmos. Sci.,* **51,** 1352–1371.

Shapiro, A., 1992: A hydrodynamical model of shear flow over semi-infinite barriers with application to density currents. *J. Atmos. Sci.,* **49,** 2293–2305.

Srivastava, R. C., 1985: A simple model of evaporatively driven downdraft: Application to microburst downdraft. *J. Atmos. Sci.,* **42,** 1004–1023.

Stevens, D. E., and P. E. Ciesielski, 1986: Inertial instability of horizontally sheared flow away from the equator. *J. Atmos. Sci.,* **43,** 2845–2856.

Thompson, R. L., R. Edwards, J. A. Hart, K. L. Elmore, and P. Markowski, 2003: Close proximity soundings within supercell environments obtained from the Rapid Update Cycle. *Wea. Forecasting,* **18,** 1243–1261.

——, C. M. Mead, and R. Edwards, 2007: Effective storm-relative helicity and bulk shear in supercell thunderstorm environments. *Wea. Forecasting,* **22,** 102–115.

Trier, S. B., C. A. Davis, D. A. Ahijevych, M. L. Weisman, and G. H. Bryan, 2006: Mechanisms supporting long-lived episodes of propagating nocturnal convection within a 7-day WRF model simulation. *J. Atmos. Sci.,* **63,** 2437–2461.

Tuttle, J. D., and C. A. Davis, 2006: Corridors of warm season precipitation in the central United States. *Mon. Wea. Rev.,* **134,** 2297–2317.

Wakimoto, R. M., 1985: Forecasting dry microburst activity over the High Plains. *Mon. Wea. Rev.,* **113,** 1131–1143.

Wallace, J. M., C. Smith, and C. S. Bretherton, 1992: Singular value decomposition of wintertime seas surface temperature and 500-mb height anomalies. *J. Climate,* **5,** 561–576.

Weisman, M. L., and J. B. Klemp, 1982: The dependence of numerically simulated convective storms on vertical wind shear and buoyancy. *Mon. Wea. Rev.,* **110,** 504–520.

——, and R. Rotunno, 2004: "A theory for strong, long-lived squall lines" revisited. *J. Atmos. Sci.,* **61,** 361–382.

——, J. B. Klemp, and R. Rotunno, 1988: Structure and evolution of numerically simulated squall lines. *J. Atmos. Sci.,* **45,** 1990–2013.

Wilks, D. S., 1995: *Statistical Methods in the Atmospheric Sciences*. Academic Press, 467 pp.

Zipser, E. J., 1982: Use of a conceptual model of the life cycle of mesoscale convective systems to improve very-short-range forecasts. *Nowcasting,* K. Browning, Ed., Academic Press, 191–221.

CORRIGENDUM

MICHAEL C. CONIGLIO, JASON Y. HWANG, AND DAVID J. STENSRUD

NOAA/National Severe Storms Laboratory, Norman, Oklahoma

(Manuscript received 3 March 2011, in final form 17 March 2011)

An error was discovered in Coniglio et al. (2010, hereafter CHS10) that led to an erroneous recommendation about how the stability of mesoscale convective system (MCS) upper-tropospheric outflow should be diagnosed. The description of inertial instability in CHS10 also needs some clarification. However, the conclusion in CHS10 that MCSs may develop more rapidly under lower inertial stability in upper levels is not affected.

The sentence on p. 3524 of CHS10 stating ''the necessary condition for inertial instability is that $\mathrm{IPV}_g < 0$'' should have read ''the necessary condition for *symmetric* instability, in a gravitationally and inertially stable atmosphere, is that $\mathrm{IPV}_g < 0$,'' where

$$\mathrm{IPV}_g = -g\frac{\partial\theta}{\partial p}(\zeta_{\theta g} + f), \tag{1}$$

and $\zeta_{\theta g}$ is the geostrophic relative vorticity along an isentropic surface. The necessary condition for inertial instability is $\zeta_{\theta g} + f < 0$. If geostrophic absolute vorticity is calculated on isentropic surfaces (as done in CHS10), and if $\partial\theta/\partial p < 0$ everywhere, then regions that are diagnosed to be inertially unstable for parcel displacements along isentropic surfaces will correspond exactly to regions that are symmetrically unstable. However, the terms ''inertial'' and ''symmetric'' should not have been used interchangeably in CHS10 without this clarification.

CHS10 found both $\zeta_{\theta g} + f$ and IPV_g to be significantly smaller for rapidly developing MCSs than for slowly developing MCSs, but IPV_g was determined to be the better discriminator. This result led to the statement starting on p. 3524 in CHS10 that ''it is important to assess the inertial stability of the environment using IPV_g, and not just the geostrophic absolute vorticity, since IPV_g takes the static stability of the atmosphere into account—a condition of weak isentropic inertial stability (i.e., small but positive IPV_g) could be met in regions with very small static stability, regardless of the magnitude of the absolute vorticity.'' However, the potential temperature from an elevation higher than the tropopause was used inadvertently to calculate static stability in a number of cases (12 of the 39 rapidly developing MCSs and 12 of the 38 slowly developing MCSs were affected). Only the static stability *below the tropopause* is relevant in this context.

To remedy the problem, an isentropic surface that was everywhere lower in elevation than the tropopause within an area bounded by $-200 \le X \le 600$ km and $-400 \le Y \le 200$ km was defined for each case, where X and Y are storm-relative coordinates denoting the geographical location of the first storms in each case (see CHS10 for details). For these modified calculations, both IPV_g and $\zeta_{\theta g} + f$ are significantly smaller for the rapidly developing MCSs in a region near the first storm's location (see Figs. 1 and 2, respectively). However, the statistical significance of the differences in IPV_g between the rapidly developing and slowly developing MCSs is slightly *lower* overall than the statistical significance of the differences in $\zeta_{\theta g} + f$ between the two subsets (cf. Figs. 1d and 2d). For example, the area enclosed by the 95% contour in Fig. 1d is substantially smaller than the area enclosed by the 95% contour in Fig. 2d. This is because the static stability in the upper troposphere was found to be slightly *larger* overall for the rapidly developing MCSs than for the slowly developing MCSs. Therefore, *the difference between using* $\zeta_{\theta g} + f$ *and* IPV_g *to diagnose the stability of the convective outflow is much smaller than originally determined in* CHS10.

However, $\zeta_{\theta g} + f$ is significantly smaller for the rapidly developing MCSs compared to the slowly developing MCSs over a relatively large area above the conditionally unstable low-level inflow region of the first storms (Fig. 2c), and these differences are actually larger

Corresponding author address: Dr. Michael C. Coniglio, National Severe Storms Laboratory, National Weather Center, Room 2234, 120 David L. Boren Blvd., Norman, OK 73072.
E-mail: michael.coniglio@noaa.gov

DOI: 10.1175/MWR-D-11-00064.1

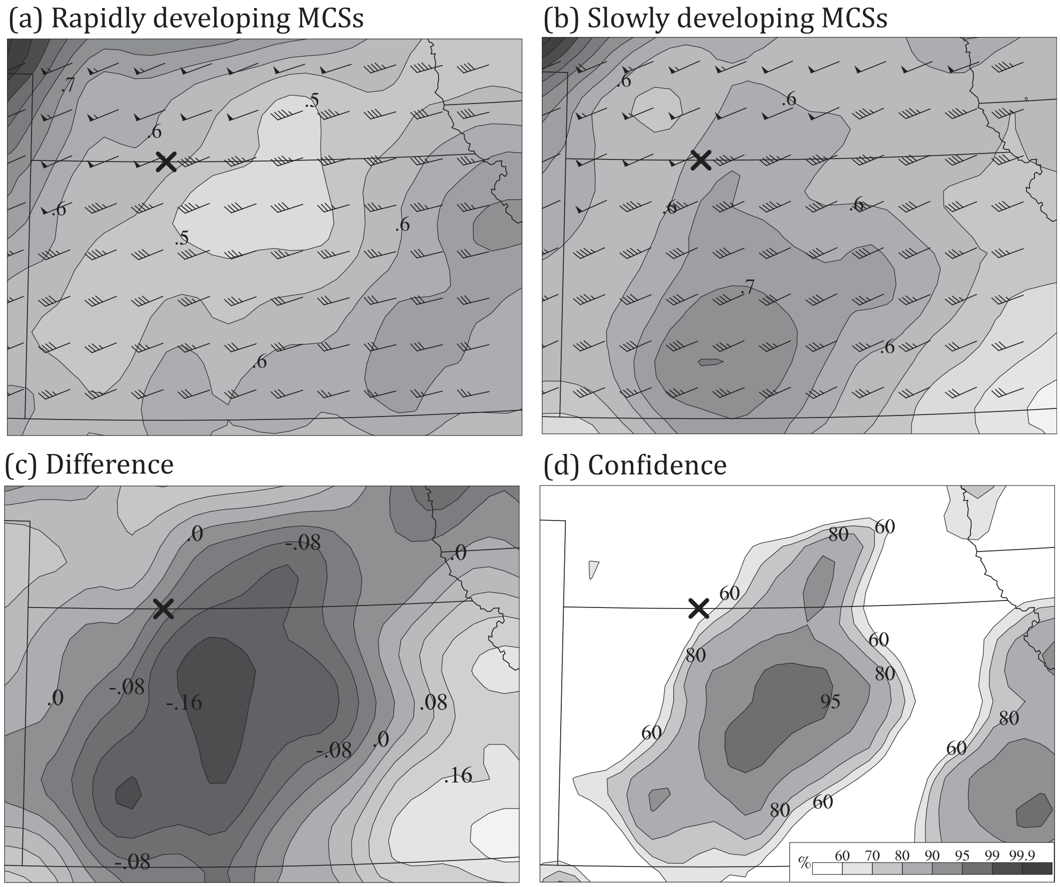

FIG. 1. The mean geostrophic potential vorticity along the normalized isentropic surface (IPV_g) for (a) the 39 rapidly developing MCSs, (b) the 38 slowly developing MCSs shaded and contoured every 0.05 PVU (1 PVU = 10^{-6} m^2 s^{-1} K kg^{-1}), (c) the difference in the means between the rapidly developing and slowly developing MCSs shaded and contoured every 0.04 PVU, and (d) the contours of the statistical significance in the differences, or the confidence that the distributions are different, based on the Wilcoxon–Mann–Whitney test (see CHS10 for details). Wind barbs depict the geostrophic wind on the normalized isentropic surface with half (full) barbs representing 2.5–7.5 (7.5–12.5) kt (1 kt = 0.5144 m s^{-1}) and pennants starting at 50 kt.

than those found for $\zeta_{\theta g} + f$ calculated along the isentropic surfaces in CHS10 (CHS10 performed calculations on surfaces spaced 5 K apart from 320 to 350 K). *Therefore, the contention that low inertial stability* (*or instability*) *could be an important factor in the speed of MCS upscale growth is upheld, and even strengthened, by these new results.*

The results in CHS10 also provided suggestions for values of IPV_g that could be used to discriminate rapidly and slowly developing MCSs in a forecast setting (see Fig. 11 of CHS10). However, these suggestions need to be modified based on the corrected results. The corrected distributions of $\zeta_{\theta g} + f$ and IPV_g shown in Fig. 3 suggest that as values of $\zeta_{\theta g} + f$ fall below 5×10^{-5} s^{-1} or values of IPV_g fall below ~0.5 in a region near and slightly equatorward of the subsequent convective development, and other factors are favorable for MCS development, then the MCS becomes increasingly likely to develop rapidly (with the caveat that these critical values may change with the grid spacing of the model output).

Acknowledgments. We thank Drs. Russ Schumacher and David Schultz for raising questions on the inertial instability section in CHS10, which led to the discovery of the error in the potential vorticity calculations.

REFERENCE

Coniglio, M. C., J. Y. Hwang, and D. J. Stensrud, 2010: Environmental factors in the upscale growth and longevity of MCSs derived from Rapid Update Cycle analyses. *Mon. Wea. Rev.*, **138,** 3514–3539.

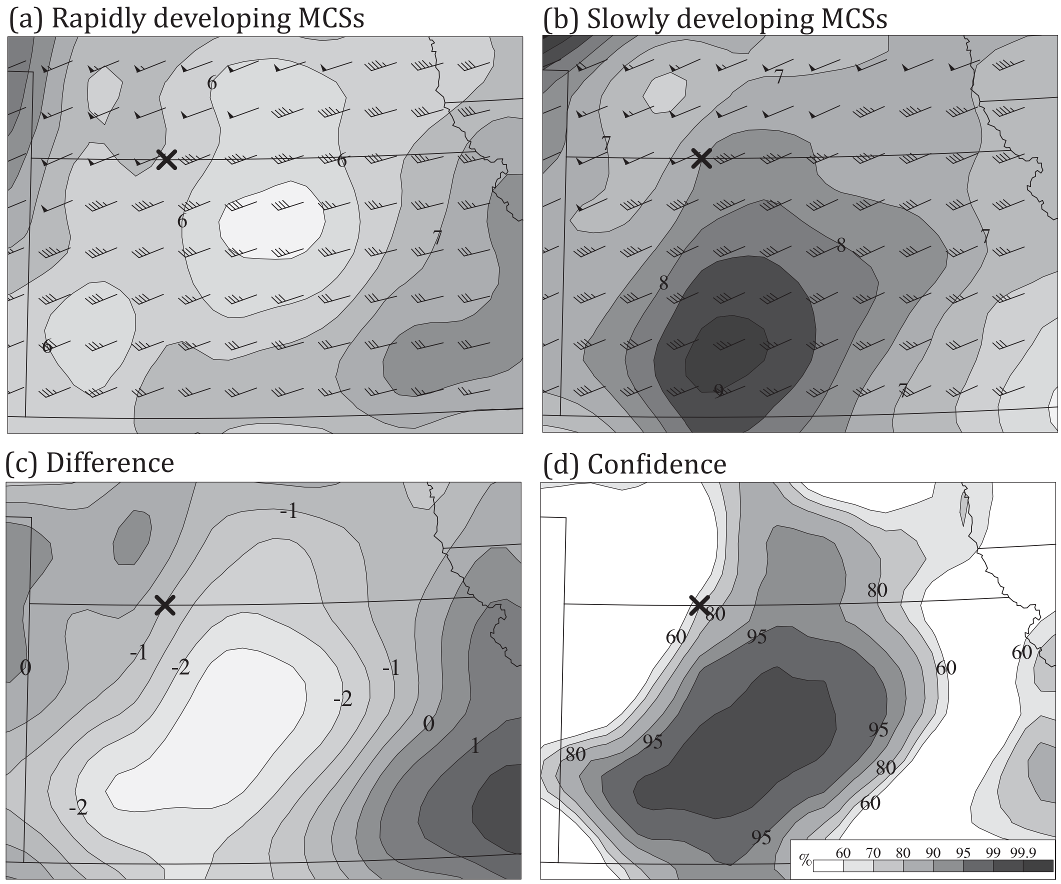

FIG. 2. (a)–(d) As in Fig. 1, but for the geostrophic absolute vorticity, $\zeta_{\theta g} + f$, shaded and contoured every 0.5×10^5 s^{-1} in (a)–(c).

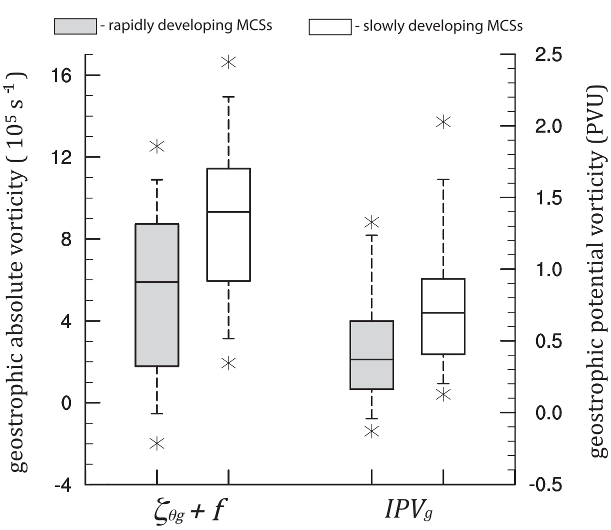

FIG. 3. Box plots representing the distribution of the geostrophic absolute vorticity, $\zeta_{\theta g} + f$, and the geostrophic potential vorticity IPV_g on the normalized isentropic surface within a 50 km by 50 km box near the maximum difference in $\zeta_{\theta g} + f$. The asterisks represent the minimum and maximum of the distributions, the dashed lines extend to the 10th and 90th percentiles, the boxes enclose the 25th and 75th percentiles, and the solid horizontal line in each box represents the median of the distribution. As done in CHS10, the distributions were calculated using the subsets with a more stringent definition of rapidly and slowly developing MCSs, namely, the 23 MCSs that took ≤4 h to develop and the 27 MCSs that took ≥8 h to develop, to emphasize the differences in the subsets.